

1 **Novel function acquired by the *Culex quinquefasciatus* mosquito D7 salivary protein**  
2 **enhances blood feeding on mammals**

3 Ines Martin-Martin, Andrew Paige, Paola Carolina Valenzuela Leon, Apostolos G. Gittis, Olivia  
4 Kern, Brian Bonilla, Andrezza Campos Chagas, Sundar Ganesan, David N. Garboczi, Eric  
5 Calvo\*

6 Laboratory of Malaria and Vector Research, National Institute of Allergy and Infectious

7 Diseases, National Institutes of Health, Rockville 20852, Maryland, USA. Correspondence and

8 requests for materials should be addressed to E.C. (email: [ecalvo@niaid.nih.gov](mailto:ecalvo@niaid.nih.gov))

## 9 Abstract

10 Adult female mosquitoes require a vertebrate blood meal to develop eggs and continue their life  
11 cycle. During blood feeding, mosquito saliva is injected at the bite site to facilitate blood meal  
12 acquisition through anti-hemostatic compounds that counteract blood clotting, platelet  
13 aggregation, vasoconstriction and host immune responses. D7 proteins are among the most  
14 abundant components of the salivary glands of several blood feeding insects. They are members  
15 of a family of proteins that have evolved through gene duplication events to encode D7 proteins  
16 of several lengths. Here, we examine the ligand binding specificity and physiological relevance  
17 of two D7 long proteins, CxD7L1 and CxD7L2, from *Culex quinquefasciatus* mosquitoes, the  
18 vector of medical and veterinary diseases such as filariasis, avian malaria, and West Nile virus  
19 infections. CxD7L1 and CxD7L2 were assayed by microcalorimetry for binding of potential host  
20 ligands involved in hemostasis, including bioactive lipids, biogenic amines, and  
21 nucleotides/nucleosides. CxD7L2 binds serotonin, histamine, and epinephrine with high affinity  
22 as well as the thromboxane A2 analog U-46619 and several cysteinyl leukotrienes, as previously  
23 described for other D7 proteins. CxD7L1 does not bind any of the ligands that are bound by  
24 CxD7L2. Unexpectedly, CxD7L1 exhibited high affinity for adenine nucleotides and  
25 nucleosides, a binding capacity not reported in any D7 family member. We solved the crystal  
26 structure of CxD7L1 in complex with bound ADP to 1.97 Å resolution. The binding pocket for  
27 ADP is located between the two domains of CxD7L1, whereas all known D7s bind ligands either  
28 within the N-terminal or the C-terminal domains. We demonstrated that these two CxD7 long  
29 proteins inhibit human platelet aggregation in *ex vivo* experiments. CxD7L1 and CxD7L2 help  
30 blood feeding in mosquitoes by scavenging host molecules that promote vasoconstriction,  
31 platelet aggregation, itch, and pain at the bite site. The novel ADP-binding function acquired by

- 32 Cx<sub>D7L1</sub> evolved to enhance blood feeding in mammals where ADP plays a key role in platelet  
33 aggregation.

## 34 1. Introduction

35 *Culex quinquefasciatus* (Diptera: Culicidae) commonly known as the southern house mosquito,  
36 is a vector of medical and veterinary importance of filaria parasites, including *Wuchereria*  
37 *bancrofti* and *Dirofilaria immitis*<sup>1,2</sup> and avian malaria parasites (*Plasmodium relictum*)<sup>3</sup>. They  
38 also can transmit several arboviruses including Rift Valley fever, West Nile, St. Louis or  
39 Western equine encephalitis viruses<sup>4,5</sup>. Adult female mosquitoes need to acquire vertebrate  
40 blood for egg development. During blood feeding, mosquito saliva is injected at the bite site and  
41 facilitates blood meal acquisition through anti-hemostatic compounds that prevent blood clotting,  
42 platelet aggregation and vasoconstriction as well as host immune responses<sup>6</sup>.

43 D7 proteins are among the most abundant components in the salivary glands of several blood  
44 feeding arthropods and are distantly related to the arthropod odorant-binding protein  
45 superfamily<sup>7,8,9,10</sup>. As mosquitoes adapted to consume different blood meals, D7 proteins  
46 evolved different biological activities to counteract the hemostatic response of their new  
47 vertebrate hosts<sup>6</sup>. The D7s belong to a multi-gene family that evolved through gene duplication  
48 events, resulting in long forms and truncated versions of a duplicated long form, known as short  
49 forms<sup>8</sup>. In addition to gene duplication, D7 proteins have undergone functional divergence,  
50 resulting in binding specialization with different affinities for host biogenic amines, as seen in  
51 *Anopheles gambiae* D7 short forms<sup>10</sup>. The D7 proteins act as kratagonists, binding and trapping  
52 agonists of hemostasis, including biogenic amines and leukotrienes (LT)<sup>8,11,12</sup>. The D7 long  
53 protein from *Anopheles stephensi* and intermediate D7 forms from the sand fly *Phlebotomus*  
54 *papatasi* have lost the capacity to bind biogenic amines but have evolved the capability to  
55 scavenge thromboxane A2 (TXA<sub>2</sub>) and LT<sup>13,14</sup>, mediators of platelet aggregation and  
56 inflammation. Interestingly, an *Aedes aegypti* D7 long protein has a multifunctional mechanism


57 of ligand binding: The N-terminal domain binds cysteinyl LT while the C-terminal domain  
58 shows high affinity to biogenic amines such as norepinephrine, serotonin, or histamine<sup>10, 11</sup>.  
59 Many authors have studied this group of proteins since the first description of a D7 salivary  
60 protein in a blood feeding arthropod<sup>15</sup>. D7 proteins play a role in blood feeding function,  
61 mosquito physiology, and alter pathogen infection or dissemination<sup>16, 17, 18, 19</sup>. Although the  
62 function of several mosquito D7 proteins including *An. gambiae* D7 short forms as well as the  
63 *Ae. aegypti* and *An. stephensi* long forms have been deciphered<sup>10, 11, 13</sup>, the role of *C.*  
64 *quinquefasciatus* D7 proteins remains unknown.

65 In this work, we expressed, purified, and biochemically characterized the two D7 long forms, L1  
66 and L2, from *C. quinquefasciatus* salivary glands. We show the different affinities for biogenic  
67 amines and eicosanoids to CxD7L2 and discovered a new function for CxD7L1. CxD7L1 has a  
68 high affinity for adenosine 5'-monophosphate (AMP), adenosine 5'-diphosphate (ADP),  
69 adenosine 5'-triphosphate (ATP), and adenosine, which are essential agonists of platelet  
70 aggregation and act as inflammatory mediators that can prevent a successful bloodmeal. CxD7L1  
71 showed no binding to biogenic amines or eicosanoids, that are previously described ligands for  
72 other D7 proteins<sup>10, 11, 13</sup>. We determined the crystal structure of CxD7L1 in complex with ADP  
73 and observed that the ADP binding pocket is located between the N-terminal and C-terminal  
74 domains. CxD7L1 is the first D7 protein to be shown to bind its ligands between the domains.  
75 We also show that CxD7L1 and CxD7L2 act as platelet aggregation inhibitors *ex vivo* supporting  
76 the hypothesis that the binding of ADP by CxD7L1 helped *C. quinquefasciatus* to evolve from  
77 blood feeding on birds, where serotonin plays a key role in aggregation, to blood feeding on  
78 mammals where ADP is a key mediator of platelet aggregation.

## 79 **2. Results**

## 80 2.1 Characterization of *Culex quinquefasciatus* CxD7L1 and CxD7L2

81 In previous studies<sup>7, 8</sup>, *Culex quinquefasciatus* salivary gland cDNA libraries were sequenced  
 82 resulting in the identification of 14 cDNA clusters with high sequence similarity to the  
 83 previously known two D7 long forms (D7clu1: AF420269 and D7clu12: AF420270) and a D7  
 84 short form (D7Clu32, AF420271). We compared the amino acid sequence of *C. quinquefasciatus*  
 85 D7 long proteins with other well characterized mosquito and sand fly D7 members, whose  
 86 function and structure have been solved. Exonic regions were conserved for all previously  
 87 studied mosquito proteins (*Culex*, *Aedes* and *Anopheles*) where the first exon corresponds to a  
 88 secretion signal peptide and the mature proteins are encoded by exons 2, 3, 4, and 5 (Fig. 1).



CxD7L1	1	DEWS-PMDPEEVAFEEAKCMEDHFGNDF---GLAEKWMKWSLAESDG-KTACYVKCLVEA
CxD7L2	1	-AWK-PFSPEETLFTYTRCMEDNAKGDL---ALAKKWMWAKLE-ADQ-KSACYAKCVLVG
AeD7	1	--MG-PFDPEEMLFIFTRCMEDNLEDGANRLPMLAKWKEWINEPVDSPATQCFGKCVLVR
AnStD7L1	1	QPWK-ALDAEQATVYVKRCYEDHLPSPGSDRKYMTLWNAWRTEPND-ITHCYAKCVLTG
CxD7L1	56	LGMYDKQ--AFQPNNIKQQYEAYKSDNGVDQTK---GDAIANELG-KIDAKDGKCESIAK
CxD7L2	54	LELFDESSKTFKGDHILEQYQKYKSYTSQDEAGVKKFQQAVQALG-TIDS--ADCLKVLQ
AeD7	58	TGLYDPVAQKFDASVIEQFKAYPELGEKSK--V---EAYANAVK-QLPSTNNDCAAVFK
AnStD7L1	59	LQIYDPQENAFKSDRIPVQYQAYKTITQSKQKEVTEYQ---KALA-AANAKSGSCVDLYN
CxD7L1	110	GFIQVNNANKGVLEKIYLLDSSVRDAIYKKN-PQIKPKGISIFRFCGKQFYQDGE---AA
CxD7L2	111	KYGPVHAQFTDVQRNVYFCKKEITDKIYNSD-STVKKRDETMFRFCERSNFKDGS---EE
AeD7	112	AYDPVHKAHKDTSKNLFHCKNKELTKGLYEKLGKDIROCKQSYEFCEKMKYYPAGSDKRQQ
AnStD7L1	115	AYLPVHNRVFNLSRQLYHCTVEGAAKIYAAM-PEIKQKGESFHAYCEKRAWKGNK--QSE
CxD7L1	166	YCNVRRKHGFSDDPKFIKHSNCTTRGMRWMKNGEMDESAILRGLHAVNENGGKDDVVKKSL
CxD7L2	167	LCTLRKKTGITTN---NHLDCLEFRGLRYLDRNGNINPDEIKRDLHFINVKDKDAVDNAL
AeD7	172	LCQTRQYTVLDDALFKEITDCVMKGIYITKDNQLDVEEVKRDVFKLVNKDTK--ALEEVL
AnStD7L1	172	WKNGRYRKLTVGSPKDAIDCIFRGLRYMDDTG-LKVDEIVRDFNLINKSELEPEVRSVL
CxD7L1	226	QNCKAKDES----KARDYKCIYDGLG-EQLFMKVLVDYIEVRSENYSYRLREATSKYDAN
CxD7L2	224	NNCKVKEAT----KATDYNCLWKPDLKDIMPVFDYREVRSESYRYFIE-NTDPYDVA
AeD7	230	NDCKSKEPSNAKEKSWHYKCLVES-SVKDDFKEAFYREVRSQIYAFNLPKNQA-YSKP
AnStD7L1	231	ASCKGS-----EAYDYYVCLVNS-RLKQHFKNAPDFHEILRSADYAYLLRGKVVY-ENPE
CxD7L1	281	AMRSKVKALDSEAKC-
CxD7L2	279	KVKEKVKKYDKDAGC-
AeD7	288	AVQSQVMEIDGKQCPQ
AnStD7L1	282	KVKEEMKLNNTTVHF-

90 **Fig. 1. Multiple sequence alignment of *C. quinquefasciatus* D7 proteins and other related sequences.**

91 Comparison of *Culex* D7 long proteins: CxD7L1 (AAL16046) and CxD7L2 (AAL16047) with *Ae. aegypti* D7:

92 AeD7 (PDB ID: 3DZT) and *An. stephensi* D7L1: AnStD7L1 (PDB ID: 3NHT). Sequences without a signal peptide

93 were aligned with Clustal Omega and refined using BoxShade server. Black background shading represents amino

94 acids involved in the eicosanoid binding of AeD7 and AnStD7L1<sup>11, 13</sup>. Red shading highlights amino acids involved

95 in biogenic amine binding for AeD7<sup>11</sup>. Position K52, highlighted with an arrow, is involved in TXA<sub>2</sub> binding<sup>13</sup>.

96 Gray shading shows conserved residues of the amino acids involved in ligands binding.

97 We named *Culex quinquefasciatus* salivary long D7 proteins CxD7L1 (AAL16046) and CxD7L2

98 (AAL16047) and characterized them by gene expression analysis and immunolocalization. To

99 determine the stage, sex, and tissue specificity of the D7 protein transcripts, qPCR experiments

100 were performed on all four larval instars, pupae, whole male, whole female, female head and

101 thorax, and female abdomen. We confirmed that both transcripts are only found in female adult

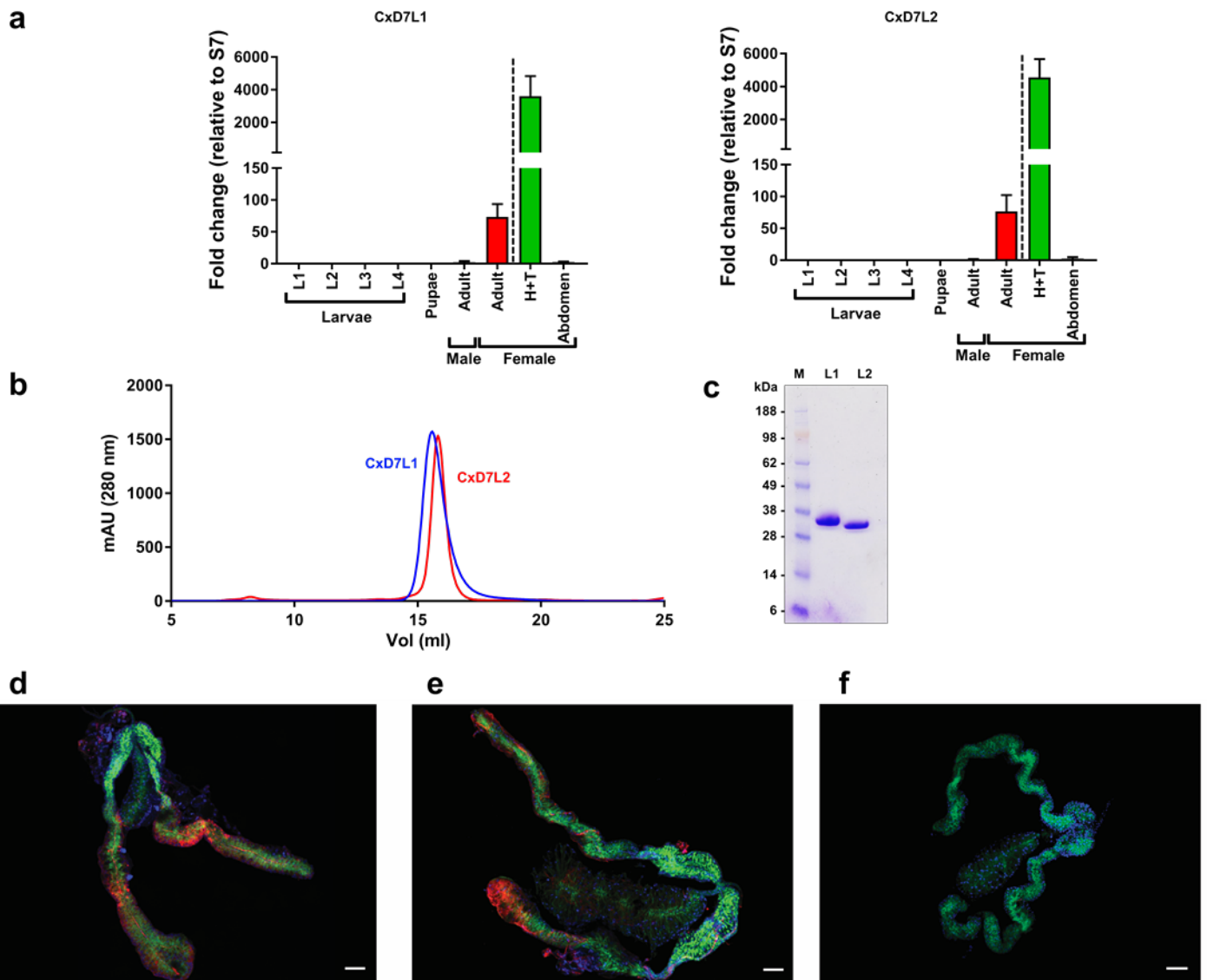
102 stages with similar levels of expression and specifically located in the head and thorax of the

103 mosquito, where the salivary glands are located. No amplification of *CxD7L1* and *CxD7L2*

104 transcripts was found in the abdomen (Fig. 2a). These results confirmed that CxD7L1 and

105 CxD7L2 expression is unique to the female salivary glands of *C. quinquefasciatus*, as previously

106 shown in *Culex* and *Anopheles* mosquitoes<sup>20, 21</sup>.



107

108 **Fig. 2. Characterization of *Culex quinquefasciatus* salivary long D7 proteins.** (a) Gene expression analysis of  
109 *CxD7L1* and *CxD7L2* transcripts in different stages of *C. quinquefasciatus* mosquitoes. Relative abundance was  
110 expressed as the fold change using the 40S ribosomal protein S7 as the housekeeping gene. Larvae stage 1 (L1),  
111 larvae stage 2 (L2), larvae stage 3 (L3), larvae stage 4 (L4), pupae, male adult (reference sample), female adult,  
112 heads and thoraxes (H+T) and abdomens from female adult mosquitoes were analyzed separately. (b) Purification of  
113 *CxD7L1* (blue line) and *CxD7L2* (red line) by size exclusion chromatography using Superdex 200 Increase 10/300  
114 GL column. (c) Coomassie-stained NuPAGE Novex 4-12% Bis-Tris gel electrophoresis of recombinant proteins  
115 *CxD7L1* and *CxD7L2* (1.5  $\mu$ g). SeeBlue Plus2 Pre-stained was used as the protein standard (M). (d and e)



116 Immunolocalization of CxD7L1 and CxD7L2 proteins in the salivary glands of *C. quinquefasciatus*. Salivary glands  
117 were incubated with rabbit IgG anti-CxD7L1 (**d**), anti-CxD7L2 (**e**) and further stained with anti-rabbit IgG Alexa  
118 Fluor 594 antibody showed in red. Proteins of interest were localized in the medial and distal regions of the lateral  
119 lobes of *C. quinquefasciatus* salivary glands. As a control, salivary glands were incubated with anti-rabbit IgG  
120 AF594 alone (**f**). Nucleic acids were stained by DAPI (blue) and the actin structure of salivary glands was stained  
121 using Phalloidin Alexa 488 (green). Scale bar = 50  $\mu$ m.

122 To investigate the biochemical and biological activities of these proteins, CxD7L1 and CxD7L2  
123 mature cDNA sequences were codon optimized for a eukaryotic cell expression system and  
124 engineered to contain a 6x-histidine tag in the C-terminal end followed by a stop codon. Both  
125 genes were subcloned into a VR2001-TOPO DNA cloning plasmid (Vical Inc) as described in  
126 Chagas *et al.*<sup>22</sup>. Recombinant CxD7L1 and CxD7L2 proteins were expressed in human  
127 embryonic kidney (HEK293) cells and purified by affinity and size exclusion chromatography  
128 (Fig. 2b). The identities of purified recombinant proteins were confirmed by N-terminal and  
129 liquid chromatography tandem mass spectrometry (LC/MS/MS sequencing). Both purified  
130 recombinant proteins migrated as single bands on Coomassie-stained precast polyacrylamide  
131 gels, and their apparent molecular weight (MW) in the gel corresponds to predicted MWs: 34.4  
132 kDa and 34.8 kDa for CxD7L1 and CxD7L2, respectively (Fig. 2c). Immunogenicity of both  
133 proteins in their recombinant forms was maintained, as they were recognized by the purified IgG  
134 antibodies from a rabbit immunized against *C. quinquefasciatus* salivary gland extract  
135 (Supplementary Fig. 1a).

136 To perform immunolocalization experiments, specific antibodies against CxD7L1 and CxD7L2  
137 were raised in rabbits. Because of the sequence similarity between these two proteins (34%  
138 identity), their antibodies showed cross-reactivity (Supplementary Fig. 1). To eliminate antibody  
139 cross-reactions and accurately identify D7 long form expression within salivary gland tissues,

140 anti-CxD7L1 IgG was pre-adsorbed with CxD7L2 and anti-CxD7L2 IgG was pre-adsorbed with  
141 CxD7L1 (Supplementary Fig. 1). Using preabsorbed antibodies allowed us to accurately localize  
142 the *Culex* D7 long proteins within the female salivary glands. As shown in Figure 2d-f, CxD7L1  
143 and CxD7L2 proteins are localized in the distal lateral and medial lobes of *C. quinquefasciatus*  
144 salivary glands, a pattern consistent with transcribed RNA of D7 long proteins in *Ae. aegypti* and  
145 *An. gambiae*<sup>23, 24</sup>.

## 146 2.2 *Culex quinquefasciatus* CxD7L1 binds adenine-nucleosides and nucleotides

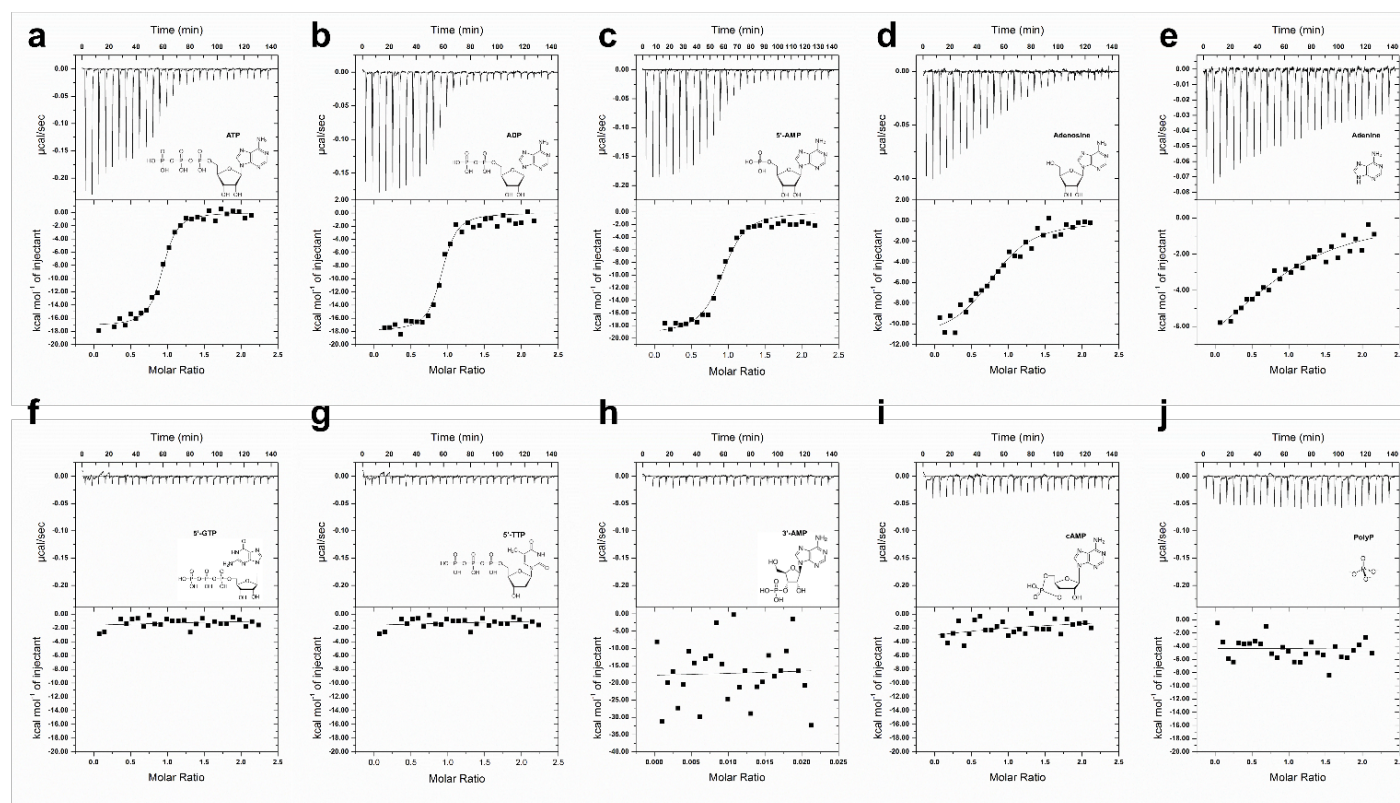
147 Previous work demonstrated that members of the D7-related protein family can bind to biogenic  
148 amines and eicosanoids<sup>10, 11, 13, 14</sup>. Scavenging these proinflammatory and hemostatic mediators  
149 may have conferred an evolutionary adaptation to blood-feeding in mosquitoes. While *Culex* D7  
150 proteins were first described in 2003<sup>21</sup> and their transcripts were sequenced a year later<sup>7</sup>, their  
151 biological activity remains unknown. The binding abilities of CxD7L1 were tested with a wide  
152 panel of pro-hemostatic compounds including biogenic amines, nucleic acids, and  
153 proinflammatory lipids using isothermal titration calorimetry (ITC). In contrast to its D7  
154 orthologs in *Aedes* and *Anopheles* mosquitoes, CxD7L1 does not bind biogenic amines such as  
155 serotonin, nor the pro-inflammatory lipids LTB<sub>4</sub> and LTD<sub>4</sub> or the stable analog of TXA<sub>2</sub>, U-  
156 46619 (Supplementary Fig. 2). However, CxD7L1 has evolved to bind adenine-nucleosides and  
157 nucleotides with high affinity (Table 1, Fig. 3), a novel function in a D7-related protein.

**Table 1 Thermodynamic parameters of *Culex quinquefasciatus* D7 proteins by isothermal calorimetry analysis**

Protein	Ligand	Stoichiometry	$\Delta H$ , cal/mol $\pm$ SE	T $\Delta S$ , cal/mol/deg	K <sub>D</sub> (nM)
CxD7L1	5'-ATP	0.91	-1.72E4 $\pm$ 277.3	-22.20	30.77
	5'-ADP	0.90	-1.80E4 $\pm$ 416.9	-25.00	32.68
	5'-AMP	0.92	-1.93E4 $\pm$ 560.8	-31.20	77.52
	Adenosine	0.85	-1.15E4 $\pm$ 668.0	-31.20	312.50
	Adenine	1.00	-9.60E3 $\pm$ 1.97E3	-5.35	1760.56

<b>CxD7L2</b>	Serotonin	1.37	$-1.63\text{E}4 \pm 171.2$	-16.50	7.46
	Histamine	0.97	$-1.31\text{E}4 \pm 579.4$	-14.00	383.14
	Epinephrine	0.94	$-5.79\text{E}4 \pm 513.8$	11.30	226.24
	LTC <sub>4</sub>	1.07	$-2.24\text{E}4 \pm 621.2$	-42.80	151.75
	LTD <sub>4</sub>	0.98	$-1.53\text{E}4 \pm 812.7$	-19.40	156.49
	LTE <sub>4</sub>	1.07	$-1.62\text{E}4 \pm 561.8$	-22.40	158.73
	Arachidonic acid	1.29	$-6.66\text{E}3 \pm 578.4$	-5.33	1083.42
U-46619	0.99	$-6.06\text{E}3 \pm 474.4$	7.58	934.58	

158



159

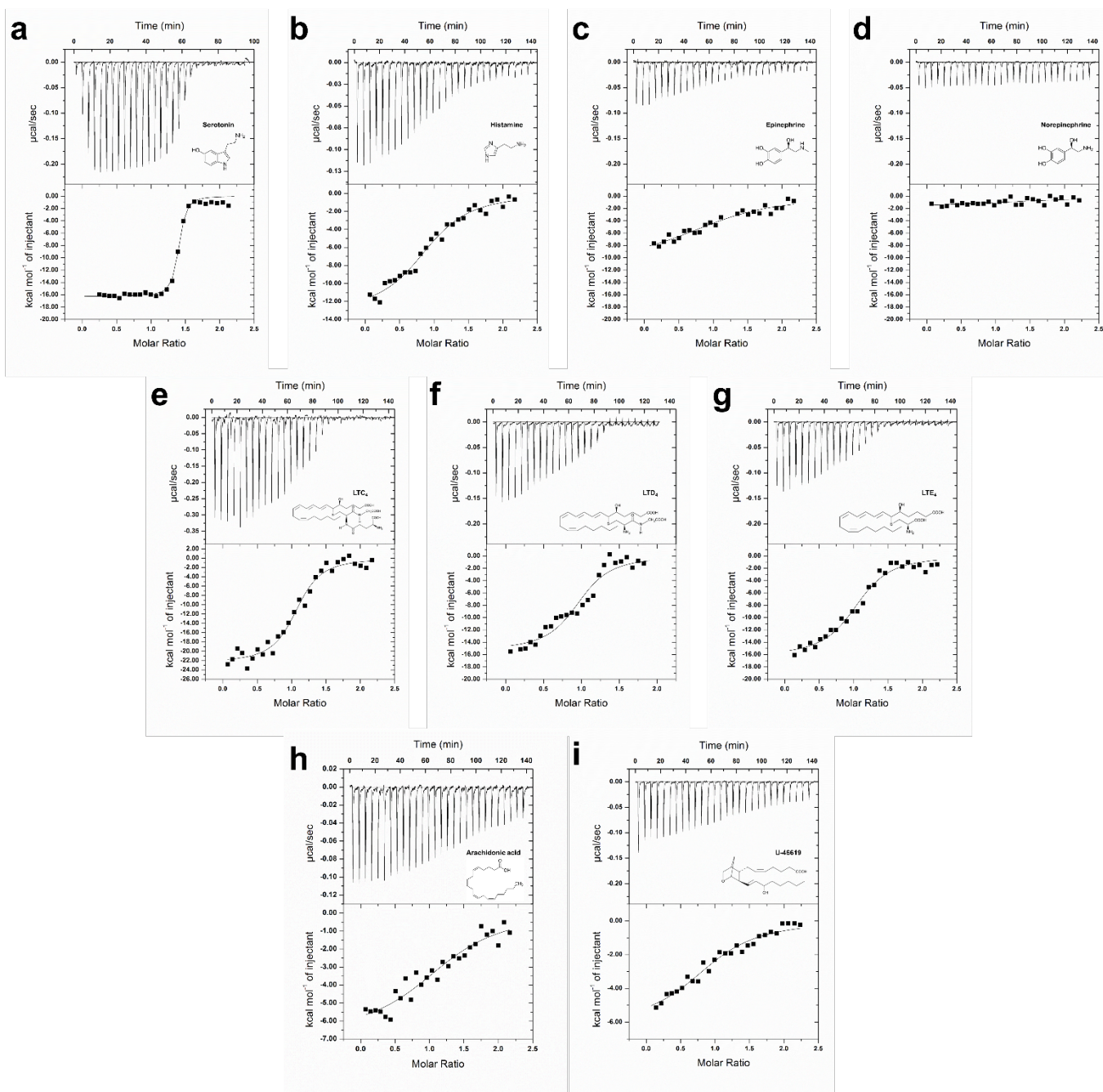
160 **Fig. 3. Binding of nucleosides and related molecules to CxD7L1 by isothermal titration calorimetry.** Binding  
 161 experiments were performed on a VP-ITC microcalorimeter. Assays were performed at 30 °C. The upper curve in  
 162 each panel shows the measured heat for each injection, while the lower graph shows the enthalpies for each injection  
 163 and the fit to a single-site binding model for calculation of thermodynamic parameters. Titration curves are  
 164 representative of at least two measurements. Panels a-e show adenine nucleosides or nucleotides that bind CxD7L1:  
 165 adenosine 5-triphosphate (a), adenosine 5-diphosphate (b), adenosine 5-monophosphate (c), adenosine (d) and  
 166 adenine (e). In panels j-f other purine and pyrimidine nucleotides and related substances showed no binding to  
 167 CxD7L1: guanosine 5-triphosphate (f), thymidine 5-triphosphate (g), adenosine 3-monophosphate (h), cyclic

168 adenosine monophosphate (i) and polyphosphate (j). The insets show the names and chemical formulas for these  
169 compounds.

170 Our biochemical characterization shows that CxD7L1 specifically binds the purine nitrogenous  
171 base adenine, its nucleoside (adenosine), and nucleotide derivatives: AMP, ADP, and ATP, with  
172 the highest affinity to ATP and ADP (Fig. 3a-e). The binding is adenine-specific, as no binding  
173 was observed with other purine or pyrimidine nucleotides such as GTP or TTP (Fig. 3f-g).  
174 Although adenine is essential for binding, CxD7L1 did not bind to adenosine 3'-monophosphate  
175 (3'-AMP) or cyclic AMP (Fig. 3h-i), highlighting the importance of the phosphate group  
176 position in binding stabilization. Interaction between CxD7L1 protein and phosphate alone was  
177 ruled out as polyphosphate (sodium phosphate glass type 45) did not bind to the protein in ITC  
178 experiments (Fig. 3j). Furthermore, CxD7L1 did not bind to inosine (Supplementary Fig. 2), an  
179 intermediate metabolite in the purine metabolic pathway.

### 180 **2.3 *Culex quinquefasciatus* CxD7L2 binds to serotonin, histamine, epinephrine, and** 181 **eicosanoids**

182 A detailed analysis of binding activities using ITC shows that CxD7L2 has comparable ligand  
183 binding capabilities as previously described in *Aedes long* and *Anopheles long* and short D7  
184 proteins (Table 1, Fig. 4)<sup>10, 11, 13</sup>. CxD7L2 tightly binds serotonin ( $K_D = 7.5$  nM) and other  
185 biogenic amines, including histamine and epinephrine, with lower affinities. It does not,  
186 however, bind norepinephrine. CxD7L2 also binds the cysteinyl leukotrienes, LTC<sub>4</sub>, LTD<sub>4</sub>, and  
187 LTE<sub>4</sub> with a stoichiometry of 1:1 all with similar binding affinities ( $K_D = 151.8$  nM, 156.5 nM  
188 and 158.7 nM, respectively, Table 1, Fig. 4). CxD7L2 also binds arachidonic acid and U-46619,  
189 the stable analog of thromboxane A<sub>2</sub>, with lower affinities ( $K_D = 1083.42$  nM and  $K_D = 934.6$   
190 nM, respectively) when compared to the cysteinyl LT. No binding to LTB<sub>4</sub> was detected.



191

192 **Fig. 4. Binding of biogenic amines and eicosanoids to CxD7L2 by isothermal titration calorimetry.** Binding  
193 experiments were performed on a VP-ITC microcalorimeter. The upper curve in each panel shows the measured  
194 heat for each injection, while the lower graph shows the enthalpies for each injection and the fit to a single-site  
195 binding model for calculation of thermodynamic parameters. Titration curves are representative of at least two  
196 measurements. Panels: serotonin (a), histamine (b), epinephrine (c) norepinephrine (d), LTC<sub>4</sub> (e), LTD<sub>4</sub> (f), LTE<sub>4</sub>

197 (g), arachidonic acid (h), and TXA<sub>2</sub> analog U-46619 (i). The insets show the names and chemical formulas for these  
198 compounds.

199 To gain insights into the mechanism of CxD7L2 binding to biogenic amines and eicosanoids, the  
200 N-terminal and C-terminal domains were independently cloned and expressed in *E. coli*. Only  
201 the C-terminal domain of CxD7L2 (CxD7L1-CT) was successfully purified and analyzed in  
202 parallel with the full-length protein by ITC. Similar to the full-length CxD7L2 protein, CxD7L2-  
203 CT binds to serotonin with high affinity ( $K_D = 1.5$  nM,  $N = 1.06$ ,  $\Delta H = 4.31E4 \pm 460$  cal/mol;  
204 for CxD7L2-serotonin see Table 1). We concluded that CxD7L2-CT is responsible for the  
205 serotonin binding capacity displayed by the full-length protein. Since we were unable to produce  
206 the CxD7L2 N-terminal domain as a non-aggregated protein, a saturation study was designed to  
207 indirectly investigate the binding specificity of this domain. For this experiment, CxD7L2  
208 protein was saturated with 50  $\mu$ M serotonin (30 min pre-incubation) and titrated with LTD<sub>4</sub> (in  
209 50  $\mu$ M of serotonin). The calculated binding parameters for CxD7L2 titrated with LTD<sub>4</sub> in the  
210 absence or presence of serotonin remained similar ( $K_D = 156.8$  nM,  $N = 0.93$ ,  $\Delta H = -2.21E4 \pm$   
211  $924.6$  cal/mol; for CxD7L2-LTD<sub>4</sub> see Table 1). These results demonstrate that lipids and  
212 biogenic amines bind to the CxD7L2 protein independently through different binding pockets,  
213 with lipids binding to the N-terminal pocket and biogenic amines to the C-terminal pocket,  
214 similar to the binding mechanism of AeD7 protein from *Ae. aegypti*<sup>11</sup>.

#### 215 **2.4 Crystal structure of *Culex quinquefasciatus* CxD7L1**

216 To further characterize the mechanism of the novel adenine nucleoside/nucleotide D7 binding,  
217 we solved the crystal structure of CxD7L1 in complex with ADP. The structure of CxD7L1 was  
218 determined by molecular replacement using Phaser by employing separate, manually constructed  
219 search models for the N-terminal and C-domains based on the crystal structure of *Anopheles*

220 *stephensi* AnStD7L1 (PDB ID: 3NHT). A crystal of CxD7L1 that belonged to I2<sub>1</sub>2<sub>1</sub>2<sub>1</sub> space  
 221 group and diffracted to 1.97 Å resolution was used to collect a data set (Table 2). The  
 222 coordinates and structure factors have been deposited in the Protein Data Bank under the  
 223 accession number 6V4C.

**Table 2 Data collection and refinement statistics**

CxD7L1-ADP Complex	
Space group	I2 <sub>1</sub> 2 <sub>1</sub> 2 <sub>1</sub>
Cell dimensions	
<i>a, b, c</i> (Å)	76.66, 84.32, 132.07
Resolution (Å)	71.07 = 1.97
I / $\sigma$ I	12.19 (2.35)
Completeness (%)	99.1 (100)
Redundancy	5.91
R-merge (%) <sup>a</sup>	6.6 (64.3)
<b>Refinement</b>	
Resolution (Å)	39.02 – 1.97
No. of reflections	29350
<i>R</i> <sub>work</sub> / <i>R</i> <sub>free</sub> (%)	21.36/23.49
No. of atoms	
Protein	2255
Ligand (Additives)	77
Water	121
Metal (Zn <sup>2*</sup> )	2
<i>B</i> -factors (Å <sup>2</sup> )	
Protein	57.51
Ligand (Additives)	60.27
Water	48.28
Metal (Zn <sup>2+</sup> )	50.96
Root mean square deviations	
Bond lengths (Å)	0.006
Bond angles (°)	0.8

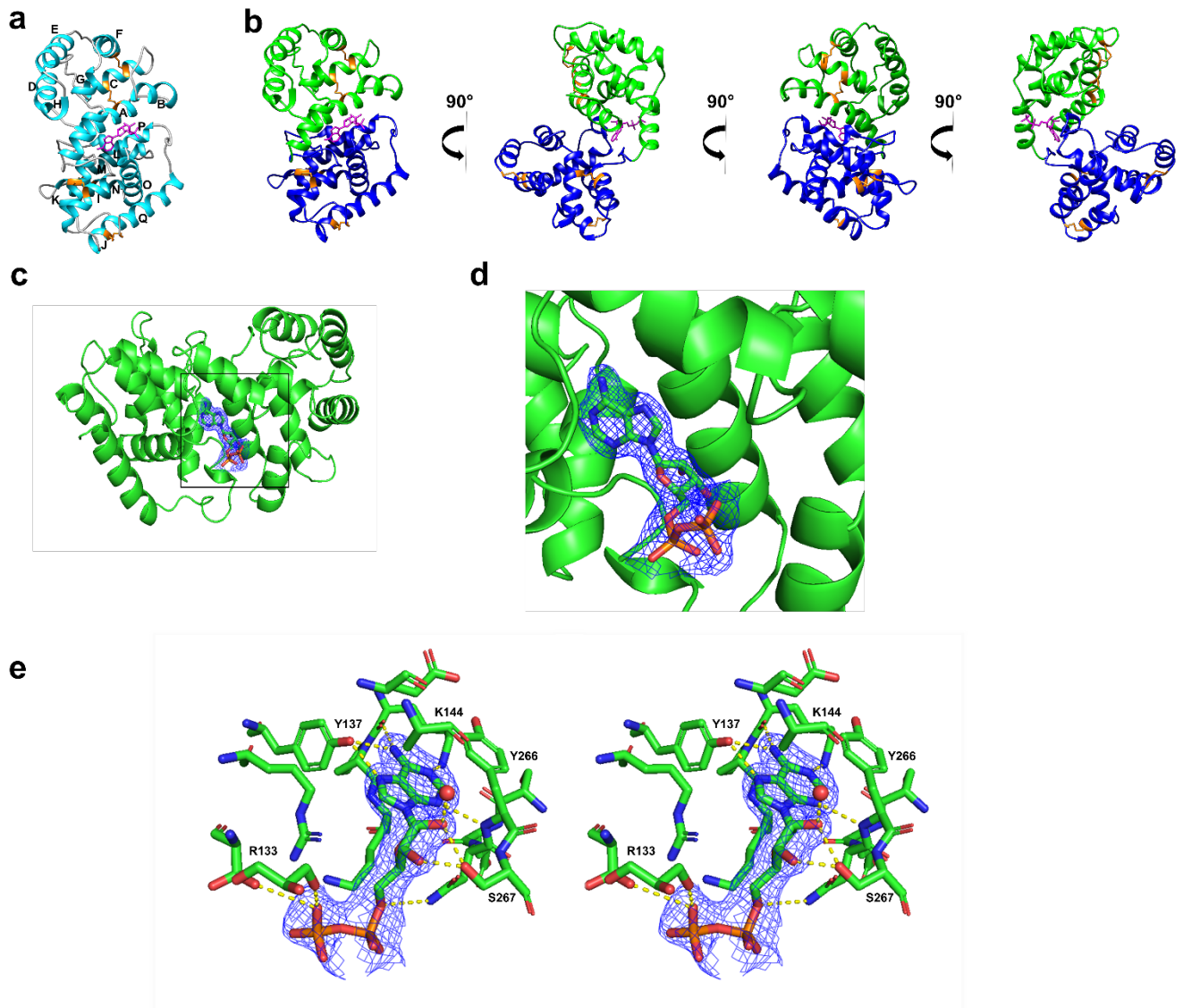
\*Values in parentheses are for highest-resolution shell.

<sup>a</sup> R-merge(I) =  $\sum_{\text{hkl}} (\sum_i |I_i(\text{hkl}) - \langle I(\text{hkl}) \rangle|) / \sum_{\text{hkl}} \sum_i I_i(\text{hkl})$ , where *I<sub>i</sub>*(hkl) is the intensity of the *i*-th observation of a reflection with indices (hkl), including those of its symmetry mates, and  $\langle I(\text{hkl}) \rangle$  is the corresponding average intensity for all *i* measurements.

225 The CxD7L1 protein fold consists of 17 helical segments stabilized by 5 disulfide bonds linking  
226 C18 with C51, C47 with C104, C154 with C186, C167 with C295 and C228 with C242 (Fig. 5a-  
227 b). The structure revealed that the ligand binding site is located between the N-terminal and C-  
228 terminal domains (Fig. 5a-e). All hydrogen bond donors and acceptors present in the adenine  
229 ring (N1, N3 and N7 are acceptors, and N6 is a donor) are interacting with the protein resulting  
230 in stable binding. The residues involved in binding ADP or stabilizing the binding pocket are  
231 R133, Y137, K144, K146, N265, Y266, S263, S267, and R271 (Fig. 5e). Residues Y137, K144  
232 and Y266 bind to the adenine ring. The hydroxyl group of Y137 forms a bidentate hydrogen  
233 bond with the N6 and N7 of the adenine ring. The carbonyl oxygen of K144 forms a hydrogen  
234 bond with the amino nitrogen N6 of the adenine ring, while the NZ of K144 is involved in 2  
235 hydrogen bonds, one with N1 from the adenine ring, and the other with the carbonyl oxygen of  
236 S263. It should be noted that the hydrogen bond with the carbonyl oxygen of S263 fixes NZ of  
237 the K144 in a position that allows it to bind the adenine ring. The amide nitrogen of Y266 binds  
238 N3 of the adenine ring and its side chain stacks partially on top of the base of ADP which  
239 provides a favorable van der Waals contribution to the CxD7L1-ADP interaction. As we go  
240 further along the ADP molecule, we find that S267 interacts strongly with and fixes the ribose  
241 ring of ADP with its hydroxyl group involved in 2 hydrogen bonds with both O2' and O3'. In  
242 addition, the ribose oxygen O2' forms a hydrogen bond with a water molecule and ND2 of N265  
243 binds to O5' of the sugar. Arginine 271 makes a hydrogen bond to N265 so that it is positioned  
244 favorably to engage in electrostatic interaction with the alpha phosphate. Lysine 146 is also in a  
245 location that can potentially be involved in electrostatic interaction with the alpha phosphate.  
246 Arginine 133 forms 2 salt bridges with the beta phosphate of ADP, with NH1 and NH2 of R133



247 binding to O1B and O3B of ADP respectively, which may explain the similar binding affinities  
248 between ATP and ADP and the lower affinity of AMP, which lacks the beta phosphate.



249

250 **Fig. 5. Structure of CxD7L1 in complex with ADP.** (a) Ribbon representation of CxD7L1-ADP structure. The 17  
251  $\alpha$ -helices are labelled A-Q. (b) Several views of CxD7L1 differing by rotations of 90 degrees around the y-axis. N-  
252 terminal and C-terminal are colored in blue and green, respectively. ADP is shown as a stick model in magenta and  
253 disulfide bonds in orange. (c) Electron density covering ADP. CxD7L1 protein is colored in green. Inset is shown in  
254 (d). Amino acid residues of CxD7L1 involved in ADP binding are colored in green (e). Stereo view of the binding

255 pocket of the CxD7L1-ADP complex showing the  $2F_o - F_c$  electron density contoured at  $1 \sigma$  covering the ligand.

256 Hydrogen bonds are colored in yellow.

257 Although the superposition of structures of CxD7L1, AeD7 (PDB:3DZT), and AnStD7L1

258 (PDB:3NHT) showed a similar overall structure (Fig. 6a), the protein sequences only share 20%

259 amino acid identity and some of the essential residues involved in the lipid and biogenic amine

260 binding are missing in CxD7L1 (Fig. 1 and Supplementary Fig. S3). Moreover, CxD7L1 showed

261 a completely different electrostatic surface potential (Coulombic Surface Coloring generated by

262 Chimera software) when compared to *Ae. aegypti* D7L and *An. stephensi* AnStD7L1, which may

263 contribute to the differences in their binding capacity. The amino acids that constitute the ADP

264 binding pocket in CxD7L1 create a strongly negative surface, showing an inverted pattern of

265 amino acid charges that completely change the nature of the binding pockets (Fig. 6b). The

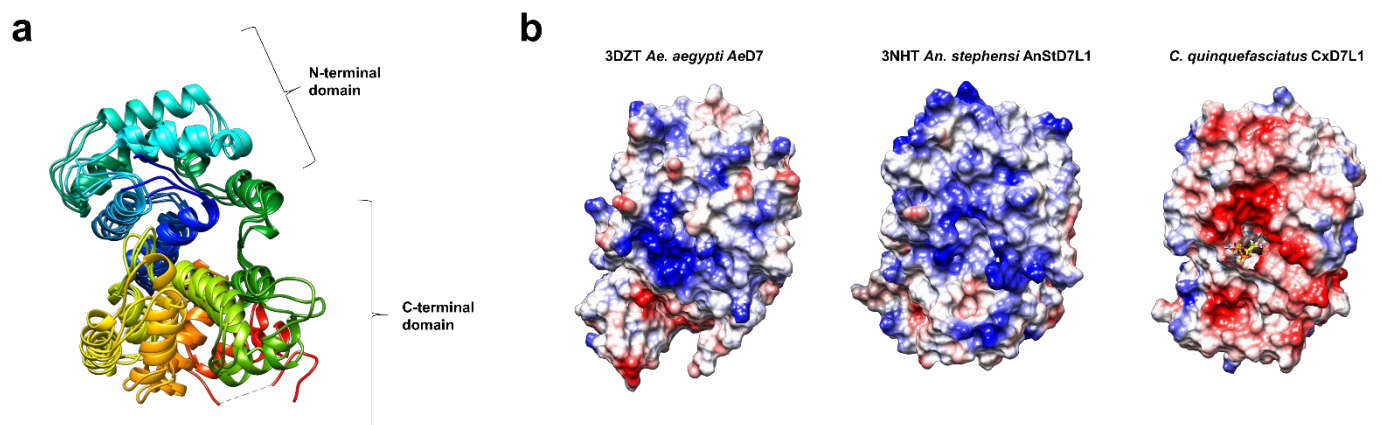
266 residues involved in ADP binding were not conserved in other D7 homologs (Fig. 1).

267 Although most of the residues were present in D7 long proteins from *Culex tarsalis*

268 (Supplementary Fig. S3) no experimental data is available showing that D7L1 from this

269 mosquito retains the ADP binding capacity.

270



271

272 **Fig. 6. Multiple sequence superposition and electrostatic potential of *Culex* D7 proteins and other related**  
273 **sequences. (a)** Superposition of CxD7L1, *Ae. aegypti* AeD7 (PDB ID: 3DZT) and *An. stephensi* AnStD7L1 (PDB

274 ID: 3NHT) shows a similar overall helix structure. Rainbow coloring pattern shows the N-terminal in blue and the

275 C-terminal in red. **(b)** Electrostatic potential of 3DZT, 3NHT and CxD7L1 generated by Coulombic Surface

276 Coloring (Chimera software) with blue being positive and red being negative. ADP is represented as a stick model.

## 277 **2.5 *Culex quinquefasciatus* CxD7L1 and CxD7L2 play a role in platelet aggregation**

278 Because CxD7 long forms bind platelet aggregation agonists such as ADP, serotonin, or the

279 TXA<sub>2</sub> analog U-46619, we examined their ability to interfere with platelet aggregation in *ex vivo*

280 experiments. At low concentrations of collagen (1 µg/mL), we saw the classical collagen

281 induction trace, where there is a delay of the platelet shape change due to the release of

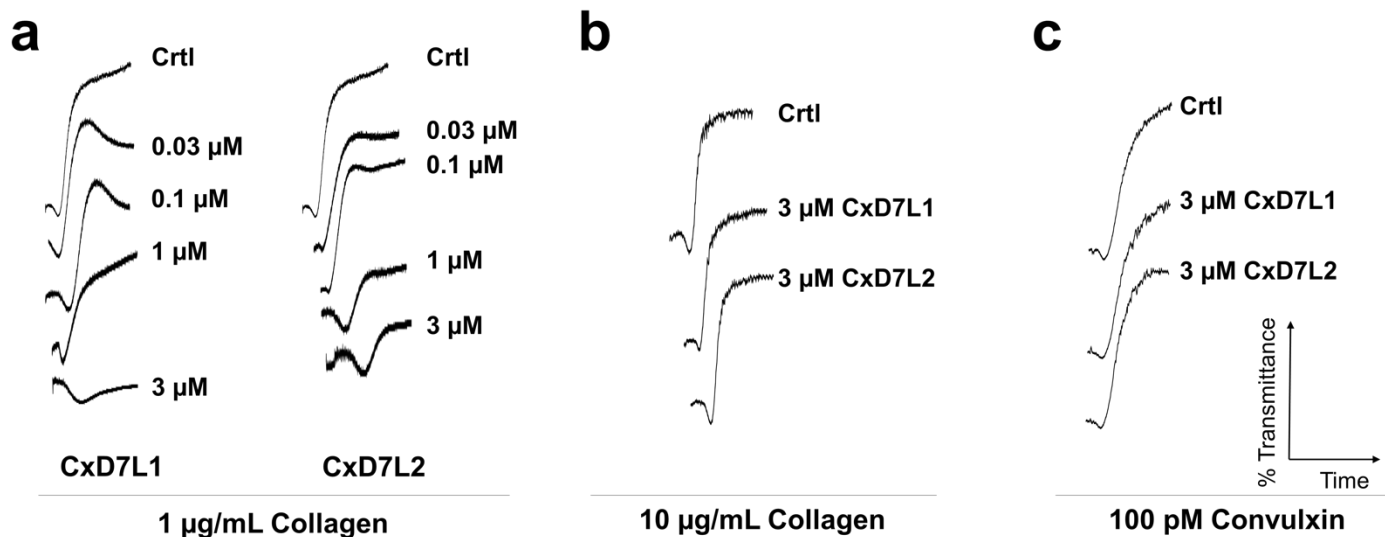
282 secondary mediators and observed as the initial decrease of light transmittance. There was a clear

283 dose-dependent inhibition of platelet aggregation by both CxD7L1 and CxD7L2 (Fig. 7a).

284 Neither CxD7L1 nor CxD7L2 interfered with platelet aggregation induced by high doses of

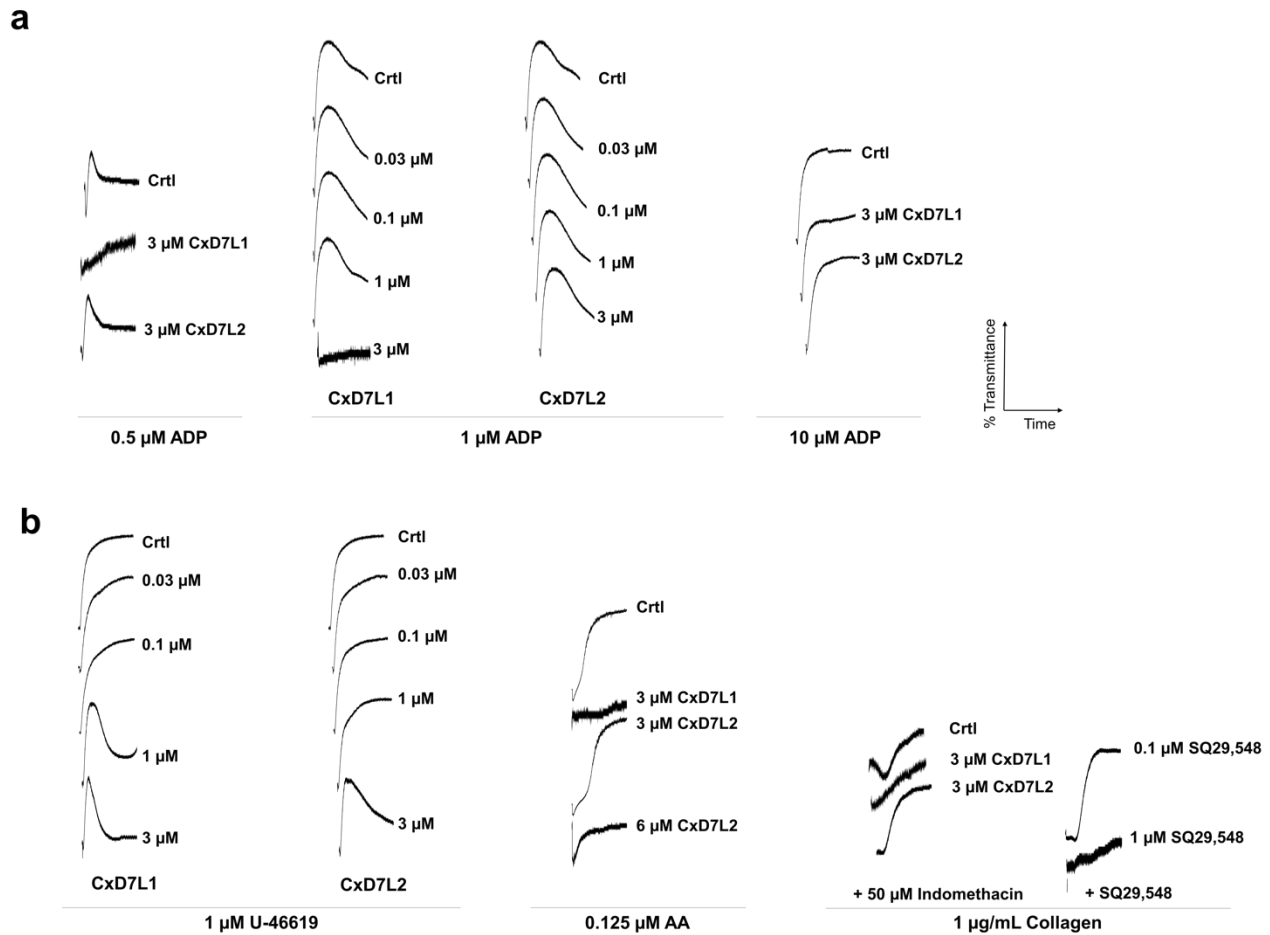
285 either collagen (Fig. 7b) or convulxin (Fig. 7c), an agonist of the platelet GPVI collagen receptor

286 which induces platelet aggregation independently of secondary mediators.



288 **Fig. 7. Effect of CxD7L1 and CxD7L2 on platelet aggregation induced by collagen or convulxin.** Prior to the  
289 addition of the agonist, platelet-rich human plasma was incubated for 1 minute with either PBS (Ctrl) or with the  
290 recombinant proteins at the concentrations shown. Aggregometer traces were measured at 37 °C from stirred  
291 platelets suspensions on a Chrono-Log platelet aggregometer model 700 for 6 min. An increase of light  
292 transmittance over time indicates platelet aggregation. **(a)** CxD7L1 and CxD7L2 concentration-dependent inhibition  
293 of platelet aggregation induced by low doses of collagen (1 µg/mL). CxD7L1 and CxD7L2 failed to inhibit platelet  
294 aggregation induced by **(b)** high doses of collagen (10 µg/mL) and **(c)** GPVI agonist convulxin (100 pM).

295 We also investigated the anti-platelet aggregation activity of CxD7L1 and CxD7L2 using ADP  
296 as an agonist. ADP plays a role in the initiation and extension of the aggregation cascade. In our  
297 studies, different concentrations of ADP were used as an agonist. When ADP was added at  
298 concentrations below the threshold for platelet aggregation (0.5 µM), only platelet shape change  
299 was observed (control trace, Fig. 8a). Preincubation of platelets with CxD7L1 prevented this  
300 shape change. With higher doses of ADP (1 µM), platelet aggregation was inhibited in the  
301 presence of 3 µM CxD7L1 (Fig. 8a). At high doses of ADP (10 µM), 3 µM of CxD7L1 was  
302 insufficient to inhibit platelet aggregation, confirming the nature of the inhibition by scavenging  
303 the mediator. The addition of CxD7L2 did not show any effect in aggregation initiated via ADP  
304 at any dose, confirming that CxD7L2 does not target ADP (Fig. 8a).



305

306 **Fig. 8. Effect of CxD7L1 and CxD7L2 on platelet aggregation induced by secondary mediators.** Prior to the  
307 addition of the agonist, platelet-rich human plasma was incubated for 1 min either with PBS (Ctrl) or with the  
308 recombinant proteins, or SQ29,548 at the concentrations shown. Aggregometer traces were measured at 37 °C from  
309 stirred platelets suspensions on a Chrono-Log platelet aggregometer model 700 for 6 min. An increase of light  
310 transmittance over time indicates platelet aggregation. **(a)** Platelet aggregation traces using different concentrations  
311 of ADP (0.5 μM, 1 μM and 10 μM) as aggregation agonist. **(b)** Platelet aggregation traces using 1 μM U-46619,  
312 0.125 μM arachidonic acid (AA) or low collagen concentration (1 μg/mL).

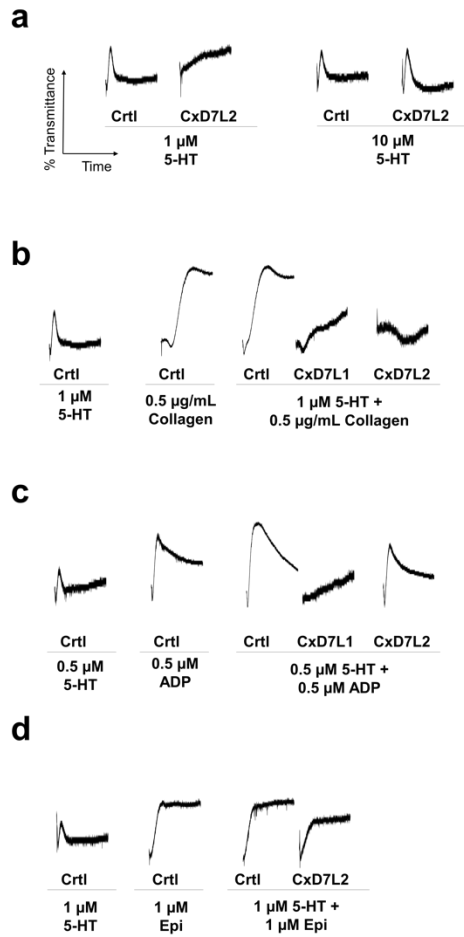
313 We also used U-46619, the stable analog of TXA<sub>2</sub> and widely accepted for platelet aggregation  
314 studies<sup>13, 14, 26, 27</sup>. When platelets are activated, TXA<sub>2</sub> is synthesized from arachidonic acid  
315 released from platelet membrane phospholipids. TXA<sub>2</sub> is an unstable compound and cannot be  
316 evaluated directly as a platelet aggregation agonist *ex vivo*. CxD7L2 inhibited U-46619-induced

317 platelet aggregation in a dose-dependent manner. However, platelet shape change requires  
318 minimal concentrations of TXA<sub>2</sub>, and it was not prevented by CxD7L2 (Fig. 8b). Shape change  
319 was only abolished in the presence of 1 μM SQ29,548, a specific antagonist of the TXA<sub>2</sub>  
320 receptor (Fig. 8b). This result is supported by our biochemical data showing that CxD7L2 binds  
321 directly to U-46619 *in vitro* (Fig. 4h). However, we do not know whether this binding is retained  
322 *in vivo*.

323 To verify that this protein binds the biological active TXA<sub>2</sub> *ex vivo*, we induced platelet  
324 aggregation with its biosynthetic precursor, arachidonic acid, so that TXA<sub>2</sub> would be released by  
325 platelets. CxD7L2 inhibited platelet aggregation induced by arachidonic acid only at high doses  
326 of protein (6 μM, Fig. 8b), most likely due to the low binding affinity observed for U-46619 and  
327 arachidonic acid (Table 1). To further investigate whether this effect was a result of a direct  
328 sequestering of TXA<sub>2</sub> by CxD7L2, we pre-incubated platelets with indomethacin, a  
329 cyclooxygenase-1 inhibitor, that prevents TXA<sub>2</sub> biosynthesis. We observed almost no inhibition  
330 of low dose collagen-induced platelet aggregation in the presence of CxD7L2 (Fig. 8b),  
331 indicating that the anti-platelet aggregation activity of CxD7L2 is mediated by TXA<sub>2</sub> binding.

332 CxD7L1 inhibits platelet aggregation induced by U-46619 in a dose-dependent manner (Fig. 8b).  
333 CxD7L1 does not bind U-46619 as shown by microcalorimetry (Supplementary Fig. S2), but it  
334 tightly binds ADP (Fig. 3b, Table 1). Platelet aggregation triggered by U-46619, arachidonic  
335 acid, and low doses of collagen is highly dependent on ADP<sup>28</sup>. As a confirmation of this  
336 dependence, CxD7L1 inhibits platelet aggregation stimulated by either U-46619 or arachidonic  
337 acid as effectively as the antagonist of the TXA<sub>2</sub> receptor SQ29,548. CxD7L1 also prevented  
338 aggregation initiated by low dose of collagen in indomethacin-treated platelets (Fig. 8b).

339 Serotonin acts as a potentiator of platelet agonists such as ADP or collagen. Alone, serotonin can  
340 initiate platelet aggregation, but in the absence of a more potent agonist, the platelets eventually  
341 disaggregate (Fig. 9a). CxD7L2 tightly binds serotonin (Fig. 4a). Therefore, the initiation of  
342 aggregation produced by serotonin was completely abolished in the presence of equimolar  
343 concentrations of the recombinant protein (Fig. 9a). However, when a higher dose of serotonin  
344 was used (10  $\mu$ M), CxD7L2 was unable to sequester all the serotonin, resulting in no observed  
345 inhibition of platelet aggregation (Fig. 9a). When serotonin and low doses of collagen were used  
346 as aggregation agonists, CxD7L1 partially prevented aggregation, presumably due to its ADP  
347 binding, while CxD7L2-serotonin binding resulted in full inhibition of platelet aggregation (Fig.  
348 9b). Serotonin also potentiated aggregation initiated by low doses of ADP (Fig. 9c). When  
349 platelets were incubated with CxD7L2, the synergistic effect of serotonin and ADP in platelet  
350 aggregation was abolished (Fig. 9c). CxD7L1, as a potent ADP-binder, completely abrogated  
351 platelet aggregation initiated by serotonin and ADP combined. In addition, CxD7L2 partially  
352 prevented aggregation initiated by serotonin and epinephrine (Fig. 9d).



353

354 **Fig. 9. Effect of CxD7L1 and CxD7L2 on platelet aggregation induced by serotonin alone or in combination**  
355 **with collagen, ADP, or epinephrine.** Prior to the addition of the agonist, platelet-rich human plasma was incubated  
356 for 1 minute either with PBS (Ctrl) or with the recombinant proteins at the concentrations shown. Aggregometer  
357 traces were measured at 37 °C from stirred platelets suspensions on a Chrono-Log platelet aggregometer model 700  
358 for 6 min. An increase of light transmittance over time indicates platelet aggregation. **(a)** Platelet aggregation traces  
359 using different concentrations of serotonin (5-HT) (1  $\mu\text{M}$  and 10  $\mu\text{M}$ ) as aggregation agonist. **(b)** Platelet  
360 aggregation traces using 5-HT in combination with collagen, **(c)** ADP or **(d)** epinephrine (Epi).

### 361 3. Discussion

362 An arthropod blood feeding event can be considered as a battle between the need of the  
363 arthropod to acquire blood and the vertebrate host response to prevent blood loss. The outcome



364 of this battle determines whether the arthropod can complete its life cycle, making a successful  
365 blood feeding event a crucial process for the fate of the invertebrate. During a bite, arthropod  
366 salivary proteins are injected into the host skin to counteract host hemostatic mediators. In this  
367 work, we characterized the structure and function of the salivary D7 long proteins from *C.*  
368 *quinquefasciatus* mosquitoes and described a novel mechanism of platelet aggregation inhibition  
369 for a D7 salivary protein.

370 CxD7L1 and CxD7L2 were found to be expressed in the distal-lateral and medial lobes of *C.*  
371 *quinquefasciatus* salivary glands. Salivary proteins have been shown to accumulate in the  
372 salivary glands forming distinct spatial patterns<sup>23</sup>. Although the relevance of distinct protein  
373 localization is not yet well understood, it supports the hypothesis of functionally-distinct regions  
374 within mosquito salivary glands. Salivary proteins related to sugar-feeding, nectar-related  
375 digestion, and bactericidal functions are localized in the proximal-lateral lobes, while proteins  
376 involved in blood-feeding, such as CxD7L1 and CxD7L2, are localized in the medial or distal-  
377 lateral lobes. More research is required to understand the implications of the salivary protein  
378 compartmentalization and viral infection of the glands.

379 D7 proteins are widely distributed in the saliva of hematophagous Nematocera, including  
380 mosquitoes, black flies, biting midges, and sand flies<sup>8</sup>. D7 salivary proteins antagonize the  
381 hemostasis mediators through a non-enzymatic, non-receptor-based mechanism by binding and  
382 sequestering several host hemostasis mediators<sup>8, 10, 11, 13, 14</sup>. This mechanism of action requires a  
383 high concentration of salivary protein at the bite site. As D7 proteins bind their ligands in a 1:1  
384 stoichiometric ratio, they must be in equimolar concentrations with the mediators, which range  
385 from 1-10  $\mu$ M for histamine, serotonin, or ADP<sup>8</sup>. This may explain why D7 salivary proteins are  
386 one of the most abundant components of the salivary glands.

387 Biogenic amines play important physiological roles in host hemostasis. Serotonin is released  
388 from platelet granules upon activation and acts as a weak platelet aggregation agonist. Serotonin  
389 and histamine increase vascular permeability and induce host sensations of pain and itch<sup>29</sup>. The  
390 catecholamines norepinephrine and epinephrine stimulate vasoconstriction by directly acting on  
391 adrenoreceptors<sup>12</sup>. Binding of biogenic amines by mosquito D7 proteins has been previously  
392 reported in the literature, highlighting the importance of removing these mediators at the bite site  
393 <sup>10, 11, 30</sup>. Binding affinities for the different amines vary, as D7 proteins have become highly  
394 specialized for specific ligands<sup>10, 11, 13, 14</sup>. CxD7L2 tightly binds serotonin and epinephrine in the  
395 same range as the short D7 proteins from *An. gambiae* and AeD7 from *Ae. aegypti*<sup>10, 11</sup>.  
396 However, it showed lower affinity for histamine and did not bind norepinephrine. Like AeD7  
397 from *Ae. aegypti*<sup>11</sup>, CxD7L2 is multifunctional and was able to bind biolipids through its N-  
398 terminal domain and biogenic amines through its C-terminal domain, as confirmed by ITC  
399 experiments. CxD7L2 binds cysteinyl leukotrienes (LTC<sub>4</sub>, LTD<sub>4</sub>, and LTE<sub>4</sub>) with similar  
400 affinities. Cysteinyl leukotrienes are potent blood vessel constrictors and increase vascular  
401 permeability<sup>31</sup>. The cysteinyl residue appears to play a role in lipid binding, as calorimetry  
402 experiments with lipids lacking a cysteinyl residue such as LTB<sub>4</sub> showed no binding. Residues  
403 involved in bioactive lipid binding were conserved between CxD7L2 and the D7 proteins from  
404 *An. stephensi* and *Ae. aegypti* (AnStD7L1 and AeD7). Interestingly, a tyrosine residue at position  
405 52 is present in *Culex* D7 long proteins and has been correlated to the ability to stabilize the  
406 binding of the TXA<sub>2</sub> mimetic (U-46619) in *An. stephensi*<sup>13</sup>. This residue is absent in the *Ae.*  
407 *aegypti* D7 protein that does not bind U-46619<sup>11</sup>. This might explain the ability of CxD7L2 to  
408 bind cysteinyl leukotrienes and U-46619. Additionally, several residues known to be involved in

409 the biogenic amine-binding were conserved in *Culex* D7 long proteins, for which the biogenic  
410 amine binding capability of CxD7L2 may be accounted.

411 Although CxD7L1 retains some amino acids involved in biogenic amine or lipid binding, ITC  
412 data showed that this protein lacks binding capacities typical of D7 proteins. Rather, CxD7L1  
413 binds adenine nucleosides and nucleotides. Our crystallographic data clearly confirms our  
414 binding results. The nature of the binding pocket demonstrates specificity for the adenine ring.  
415 The hydrogen bonds between the adenine ring and residues Y137, K144, and Y266 determine  
416 the specificity for adenine and the lack of binding to other nucleotides with other nitrogenous  
417 bases (5'-GTP, 5'-TTP). Similarly, S267 and N265 of CxD7L1 are involved in binding to the  
418 ribose, which is possible when the phosphate group occupies position 5' but not position 3' or  
419 the cyclic form, as shown by calorimetry experiments. Arginine 133 binds to the oxygen of the  
420 beta phosphate of ADP which may explain the similar binding affinities for both ATP and ADP  
421 while affinity for AMP is lower as it lacks the beta phosphate.

422 CxD7 proteins scavenge biogenic amines, LTs, and ADP released at the bite site, and thus  
423 prevent hemostasis by inhibiting several simultaneous signaling cascades. Here, we have focused  
424 on their contributions in preventing platelet aggregation. Platelet aggregation occurs within  
425 seconds of tissue injury, restricting blood flow and creating a platelet plug that reduces blood  
426 feeding success. Exposure of circulating platelets to collagen from the subendothelial matrix or  
427 thrombin leads to the formation of a platelet monolayer that supports subsequent adhesion of  
428 activated platelets to each other<sup>12, 32</sup>. At low concentrations of collagen, ADP and TXA<sub>2</sub> play an  
429 important role on the extension and amplification step of the platelet plug formation. Upon  
430 platelet activation, mediators secreted by platelets bind to G protein-coupled receptors in platelet  
431 membranes, rapidly amplifying the aggregation signal in a positive feedback response<sup>33</sup>.

432 However, at high concentrations, collagen acts as a strong agonist of the GPVI receptor on  
433 platelet surface, which induces platelet aggregation in an independent manner of ADP or TXA<sub>2</sub>  
434 secretion<sup>32</sup>. Both CxD7L1 and CxD7L2 proteins showed a potent inhibitory effect on platelet  
435 aggregation, explained by distinct mechanisms. CxD7L2 inhibits platelet aggregation in the  
436 classical mechanism observed in other eicosanoid-scavenging salivary proteins<sup>13, 14, 26, 34, 35</sup>.  
437 CxD7L2 inhibits low dose collagen-induced platelet aggregation in a dose dependent manner but  
438 did not affect aggregation induced by high doses of collagen or convulxin. These findings  
439 indicate that CxD7L2's inhibitory effect on platelet aggregation is dependent on secondary  
440 mediators and does not interfere with collagen directly. CxD7L2 showed a low binding affinity  
441 for U-46619, the stable analog of TXA<sub>2</sub> (934.58 nM), and its precursor, arachidonic acid  
442 (1083.42 nM) which might explain the high doses needed to neutralize the aggregation induced  
443 by arachidonic acid. CxD7L2 also binds serotonin and epinephrine which act as weak platelet  
444 agonists alone, but are important as they reduce the threshold concentrations of other agonists for  
445 platelet aggregation, as previously observed for the biogenic amine-binding protein from the  
446 triatomine *Rhodnius prolixus*<sup>36</sup>.

447 In contrast, we have demonstrated the novel mechanism by which CxD7L1 inhibits platelet  
448 aggregation, never reported before in the D7 protein family. CxD7L1 inhibited aggregation  
449 induced by low doses of ADP or collagen in a dose-dependent manner. Platelet aggregation  
450 induced by low doses of collagen is known to be highly dependent on ADP release from platelet  
451 granules, as platelets treated with apyrase or ADP receptor antagonists poorly respond to these  
452 agonists<sup>37, 38</sup>. CxD7L1 showed an inhibitory effect on aggregation triggered by the TXA<sub>2</sub>  
453 pathway, as it attenuated aggregation induced by both U-46619 and arachidonic acid, the TXA<sub>2</sub>  
454 precursor, which suggests that CxD7L1 interacts with TXA<sub>2</sub>. However, we showed CxD7L1

455 does not bind TXA<sub>2</sub> through ITC and aggregation studies, ruling out the direct interaction  
456 between CxD7L1 and TXA<sub>2</sub>. It is known that aggregation through TXA<sub>2</sub> is linked to ADP  
457 signaling<sup>39</sup>. This observation agrees with a previous description of a *R. prolixus* aggregation  
458 inhibitor 1 (RPAI-1) which binds ADP and interferes with TXA<sub>2</sub> pathways<sup>28</sup>. Taken all together,  
459 we demonstrated that CxD7L1 inhibits platelet aggregation by sequestering ADP, which is  
460 released from platelet dense granules upon platelet activation promoting a stable platelet  
461 response<sup>32, 33, 40</sup>. By removing secreted ADP from the vicinity of the platelet, CxD7L1 prevents  
462 ADP from performing its role of platelet propagation.

463 Adenine nucleotides and derivatives play an important role in vascular biology and immunology  
464 at the mosquito bite site. ATP and ADP induce constriction of blood vessels and ADP acts as a  
465 potent mediator of platelet aggregation in mammals. Metabolism of ATP and ADP would lead to  
466 the production of AMP by apyrases that would be further metabolized to adenosine by 5-  
467 nucleotidase. Apyrases have been found in the saliva of most blood feeding arthropods studied  
468 so far<sup>12</sup>. The ability of CxD7L1 to scavenge ATP and ADP may compensate for the low salivary  
469 apyrase activity detected in *C. quinquefasciatus* compared to *Ae. aegypti*<sup>41</sup>. CxD7L1 also binds  
470 and scavenges adenosine. Although adenosine causes vasodilation and inhibits platelet  
471 aggregation, it also stimulates pain receptors and triggers pain and itch responses by inducing  
472 mast cell degranulation. Pain and itch may alert the host to the presence of a biting mosquito,  
473 preventing a successful blood meal<sup>42</sup>.

474 Arthropods underwent multiple independent evolutionary events to adapt to consume blood  
475 meals from different or new hosts. This independent evolutionary scenario has led to a great  
476 variety of salivary protein families that have acquired different functions related to blood-  
477 feeding. Gene duplication is an important mechanism for the evolution of salivary proteins.

478 Duplication of D7 genes may have been advantageous in providing greater amounts of D7  
479 proteins at the bite site to counteract high concentrations of host mediators<sup>43</sup>. Gene duplication  
480 combined with the pressure of the host hemostatic and immune responses may have led to  
481 functional divergence as observed in the D7 short proteins from *An. gambiae* and their  
482 specialization towards different biogenic amines<sup>10</sup>. The D7 protein family is polygenic in all  
483 Nematocera so far studied<sup>44</sup>. In *C. quinquefasciatus*, D7 genes are also a result of gene  
484 duplication events, given the number of genes that encode D7 proteins and their location in the  
485 genome on chromosome 3<sup>45</sup>. *Culex quinquefasciatus* mosquitoes are traditionally considered  
486 bird-feeders that later adapted to mammalian blood-feeding. They are increasingly recognized as  
487 important bridge vectors, vectors that acquire a pathogen from an infected wild animal and  
488 subsequently transmit the agent to a human, based on studies that examine host preference,  
489 vector/host abundance, viral infection rates, and vector competence<sup>46</sup>. *Culex quinquefasciatus*  
490 contain potent salivary proteins that counteract bird thrombocytes aggregation mediators such as  
491 serotonin and platelet activation factor (PAF). We have demonstrated that CxD7L2 tightly binds  
492 serotonin while Ribeiro *et al.* demonstrated that PAF phosphorylcholine-hydrolase inhibits PAF  
493 enzymatically<sup>46</sup>. Thrombocytes are not responsive to ADP<sup>47, 48</sup>, but ADP is an important  
494 mediator of platelet aggregation in mammals. We hypothesize that the novel function of ADP-  
495 binding by CxD7L1 protein has arisen from the selective pressure of mammalian hemostatic  
496 responses. This acquired D7-ADP-binding function may have provided an advantageous trait in  
497 *C. quinquefasciatus* mosquitoes that helped them to adapt to blood-feeding on mammals. *Culex*  
498 *tarsalis* mosquitoes prefer to feed on birds but will readily feed on mammals in the absence of  
499 their preferred host<sup>49</sup>. An alignment between CxD7L1 and *C. tarsalis* D7 long proteins showed  
500 that most of the residues involved in ADP binding are conserved in *C. tarsalis*, suggesting that

501 D7 proteins that bind ADP may be widespread in the genera *Culex*. More studies are necessary  
502 to confirm this hypothesis.

503 In conclusion, we determined the binding capabilities of the CxD7L1 and CxD7L2 proteins and  
504 demonstrated their role in inhibiting human platelet aggregation through different mechanisms of  
505 action. We identified a novel function of ADP-binding in the well-characterized D7 protein  
506 family. Moreover, the structure of the complex CxD7L1-ADP was solved, showing a different  
507 binding mechanism for a D7 with the binding pocket located between the N-terminal and C-  
508 terminal domains whereas most D7s bind ligands within one of these two respective domains.  
509 These proteins help blood feeding in mosquitoes by scavenging host molecules at the bite site  
510 that promote vasoconstriction, platelet aggregation, itch, and pain. Accumulation of these  
511 proteins in the salivary glands of females confers an evolutionary advantage for mosquito blood  
512 feeding on mammals.

## 513 **4. Methods**

### 514 **4.1 Ethics statement**

515 Public Health Service Animal Welfare Assurance #A4149-01 guidelines were followed  
516 according to the National Institute of Allergy and Infectious Diseases (NIAID), National  
517 Institutes of Health (NIH) Animal Office of Animal Care and Use (OACU). These studies were  
518 carried out according to the NIAID-NIH animal study protocol (ASP) approved by the NIH  
519 Office of Animal Care and Use Committee (OACUC), with approval ID ASP-LMVR3.

### 520 **4.2 Mosquito rearing and salivary gland dissection**

521 *Culex quinquefasciatus* mosquitoes were reared in standard insectary conditions at the  
522 Laboratory of Malaria and Vector Research, NIAID, NIH (27 °C, 80% humidity, with a 12-h

523 light/dark cycle) under the expert supervision of Andre Laughinghouse, Kevin Lee, and Yonas  
524 Gebremicale. The mosquito colony was initiated from egg rafts collected in Hilo, Hawaii, US,  
525 and maintained at NIH since 2015. Salivary glands from sugar-fed 4 to 7-day old adult  
526 mosquitoes were dissected in PBS pH 7.4 using a stereomicroscope. Salivary gland extract  
527 (SGE) was obtained by disrupting the gland wall by sonication (Branson Sonifier 450). Tubes  
528 were centrifuged at  $12,000 \times g$  for 5 min and supernatants were kept at  $-80^{\circ}\text{C}$  until use.

### 529 **4.3 CxD7L1 and CxD7L2 gene expression pattern**

530 *Culex quinquefasciatus* larvae (stages L1 to L4 categorized by age and size), pupae, and adults  
531 (male and female) were collected and kept in Trizol reagent (Life Technologies). Additionally,  
532 female adults were dissected, head and thorax were separated from abdomens, and independently  
533 analyzed. In all cases each sample consisted of 10 specimens. Total RNA was isolated with  
534 Trizol reagent following the manufacturer instructions (Life Technologies). cDNA was obtained  
535 with the QuantiTect Reverse Transcriptase Kit (Qiagen), from 1  $\mu\text{g}$  of starting RNA. Nanodrop  
536 ND-1000 spectrophotometer was used to determine all concentrations and  $\text{OD}_{260/280}$  ratios of  
537 nucleic acids. qPCR was carried out as previously described<sup>50</sup>. Specific primers to target  
538 CxD7L1 and CxD7L2 genes were designed (CxD7L1-F: 5'-ACGGAAGCATGGTTTTTCAG-  
539 3', CxD7L1-R: 5'-GGATTGCAGATTCGTCCATT-3', CxD7L2-F: 5'-  
540 CCACGAACAACAACCATCTG-3', CxD7L2-R: 5'-CACGCTTGATTTTCATCAGGA-3').  
541 Briefly, in a final volume of 20  $\mu\text{l}$ , reaction mix was prepared with 2X SsoAdvanced Universal  
542 SYBR Green Supermix (Bio-Rad), 300 nM of each primer, and 100 ng of cDNA template. Two  
543 biological replicates were tested. All samples were analyzed in technical duplicates and non-  
544 template controls were included in all qPCR experiments as negative controls. qPCR data were  
545 manually examined and analyzed by the  $\Delta\Delta\text{Ct}$  method.  $\Delta\text{Ct}$  values were obtained by normalizing



546 the data against *C. quinquefasciatus* 40S ribosomal protein S7 transcript (AF272670; CxS7-F:  
547 5'-GTGATCAAGTCCGGCGGTGC-3' and CxS7-R: 5'-GCTTCAGGTCCGAGTTCATCTC-  
548 3') as the reference gene. Male adult samples were chosen as controls for the  $\Delta\Delta C_t$  values.  
549 Relative abundance of genes of interest was calculated as  $2^{-\Delta\Delta C_t}$ .

#### 550 **4.4 Cloning, expression and purification of recombinant proteins**

551 CxD7L1 and CxD7L2 coding DNA sequences (AF420269 and AF420270) were codon-  
552 optimized for mammalian expression and synthesized by BioBasic Inc. VR2001-TOPO vectors  
553 containing CxD7L1 and CxD7L2 sequences (Vical Incorporated) and a 6x-histidine tag were  
554 transformed in One Shot TOP10 chemically competent *E. coli* (Invitrogen). FreeStyle 293-F  
555 mammalian cells were transfected with sterile plasmid DNA, prepared with EndoFree plasmid  
556 MEGA prep kit (Qiagen, Valencia, CA), at the SAIC Advance Research Facility (Frederick,  
557 MD), and supernatants were collected 72 h after transfection. Recombinant proteins were  
558 purified by affinity chromatography followed by size-exclusion chromatography, using Nickel-  
559 charged HiTrap Chelating HP and Superdex 200 10/300 GL columns, respectively.

560 To determine the crystal structure, recombinant CxD7L1 was produced in *E. coli*. The CxD7L1  
561 coding DNA sequence was amplified by PCR from cDNA of *C. quinquefasciatus* salivary glands  
562 and was cloned in pET-17b plasmid and expressed in BL21 pLysS cells (Invitrogen). Protein  
563 expression was carried out as previously described<sup>51</sup>. Inclusion bodies were refolded using 200  
564 mM arginine, 50 mM Tris, 1 mM reduced glutathione, 0.2 mM oxidized glutathione, 1 mM  
565 EDTA, pH 8.0. Bacterial CxD7L1 was purified by size exclusion chromatography, using a  
566 HiPrep 16/60 Sephacryl S-100 HR column, followed by cation exchange chromatography with a  
567 HiPrep SP FF 16/10 column. A last step of analytical size exclusion chromatography was  
568 performed using a Superdex 200 10/300 GL column with 25 mM Tris, 50 mM NaCl pH 7.4. All

569 HPLC columns were obtained from GE Healthcare Life Science, Piscataway, NJ. All purified  
570 proteins were separated in a 4-20% NuPAGE Tris-glycine polyacrylamide gel and visualized by  
571 Coomassie stain. Protein identity was verified by Edman degradation at the Research  
572 Technologies Branch, NIAID, NIH.

#### 573 **4.5 Polyclonal antibody production**

574 Polyclonal antibodies against CxD7L1 and CxD7L2 were raised in rabbits. Immunization of  
575 rabbits was carried out in Noble Life Science facility according to their standard protocol  
576 (<http://www.noblelifesci.com/preclinical-drug-development/polyclonal-antibody-production/>).  
577 Rabbit sera were shipped to our laboratory where purification of IgG was performed by affinity  
578 chromatography using a 5-ml HiTrap protein A HP column following manufacturer's  
579 instructions (GE Healthcare, Piscataway, NJ). Purified IgG protein concentration was determined  
580 by Nanodrop ND-1000 spectrophotometer. Additionally, antibodies against *C. quinquefasciatus*  
581 salivary gland extract were raised in rabbits. Levels of specific antibodies were determined by  
582 ELISA according to Chagas *et al.*<sup>52</sup>

#### 583 **4.6 Western blot**

584 *Culex quinquefasciatus* salivary gland extracts (2.5 µg) and 100 ng of CxD7L1 and CxD7L2  
585 were separated by NuPAGE. Proteins were transferred to a nitrocellulose membrane (iBlot,  
586 Invitrogen) that was blocked overnight at 4 °C with blocking buffer: TBS containing 5% (w/v)  
587 powdered non-fat milk. Purified anti-CxD7L1 and anti-CxD7L2 IgG antibodies were diluted in  
588 blocking buffer (0.5 µg/ml) and incubated for 90 min. Goat anti-rabbit conjugated to alkaline  
589 phosphatase (Sigma) diluted in blocking buffer (1:10,000) was used as a secondary antibody and

590 immunogenic bands were developed by the addition of BCIP/NBT substrate (Promega). The  
591 reaction was stopped with distilled water.

#### 592 **4.7 Immunolocalization of CxD7L1 and CxD7L2**

593 *Culex quinquefasciatus* salivary glands were dissected in PBS, transferred to a well plate, and  
594 fixed with 4% paraformaldehyde (Sigma) for 30 min at room temperature. Tissues were washed  
595 3 times for 10 min each with 1x PBS to remove paraformaldehyde and then blocked with 2%  
596 BSA, 0.5% Triton X-100, 1x PBS pH 7.4 overnight at 4 °C. Glands were washed 3 times with  
597 PBS to remove Triton X-100 and were transferred to clean wells to which 200 µl of 1 µg/ml pre-  
598 adsorbed antibodies against either CxD7L1 or CxD7L2 (raised in rabbits and diluted 1:1000 in  
599 2% BSA 1x PBS) were added. Glands incubated in 2% BSA 1x PBS served as a negative  
600 control. Plate wells were covered and incubated overnight at 4 °C. Primary antibodies were  
601 removed by 3 washes with 2% BSA 1x PBS and incubated with 2 µg/ml anti-rabbit IgG Alexa  
602 Fluor 594 (Thermo Fisher) for 2 h in the dark at 4°C. Conjugate was removed by 3 additional  
603 washes with 1x PBS. DNA was stained with 1 µg/mL DAPI (Sigma D9542) and actin with 0.04  
604 µg/mL Phalloidin Alexa 488 (Invitrogen) for 20 min. Glands were washed three times with PBS  
605 and transferred to glass slides containing droplets of PBS. PBS was removed without drying the  
606 glands, and tissues were mounted using a coverslip coated with 25 µl Prolong Gold mounting  
607 medium. Slides were covered and left to dry at room temperature and then stored at 4 °C. Bright  
608 field and fluorescent images were acquired in a Leica Confocal SP8 microscope with a 63x  
609 objective using Navigator tool. Images were processed with Imaris software version 9.2.1 and  
610 postprocessing was carried out in Fiji ImageJ for representative purposes.

#### 611 **4.8 Isothermal titration calorimetry (ITC)**

612 Thermodynamic binding parameters of CxD7L1 and CxD7L2 to several pro-hemostatic ligands  
613 were tested using a Microcal VP-ITC microcalorimeter. The panel of substances tested included  
614 several nucleosides/nucleotides or derivatives (ATP, ADP, 5'-AMP, 3'-AMP, cyclic AMP,  
615 adenosine, GTP, TTP, inosine, sodium polyphosphate, Sigma-Aldrich), biogenic amines  
616 (epinephrine, norepinephrine, histamine, serotonin, Sigma-Aldrich), and pro-inflammatory/pro-  
617 hemostatic lipid compounds (LTB<sub>4</sub>, LTC<sub>4</sub>, LTD<sub>4</sub>, LTE<sub>4</sub>, arachidonic acid, and the stable analog  
618 of TXA<sub>2</sub>: U-46619, Cayman Chemicals). Ligands and protein solutions were prepared in 20 mM  
619 Tris-HCl pH 7.4, 150 mM NaCl (TBS) at 30 and 3 μM, respectively. Lipids ligands were  
620 prepared by evaporating the ethanol or chloroform solvent to dryness under a stream of nitrogen.  
621 Lipid ligands were further dissolved in TBS and sonicated for 10 min (Branson 1510) to ensure  
622 dissolution. Lipid ligands were used at 50 μM of ligand and 5 μM of protein. Injections of 10 μl  
623 of ligand were added to the protein samples contained in the calorimeter cell at 300 sec intervals.  
624 Experiments were run at 30 °C. Thermodynamic parameters were obtained by fitting the data to  
625 a single-site binding model in the Microcal Origin software package. For saturation studies,  
626 CxD7L2 protein was pre-incubated with 50 μM serotonin for 30 min and titrated with LTD<sub>4</sub>.

#### 627 **4.9 CxD7L1 Crystallization, data collection and structure determination**

628 Purified protein was incubated overnight at 4°C with 1.2 times molar excess of ADP. Crystals  
629 were obtained using the hanging drop-vapor diffusion method with 0.01 M Zinc sulfate  
630 heptahydrate, 0.1 M MES monohydrate pH 6.5, and 25% v/v Polyethylene glycol monomethyl  
631 ether 550 (Crystal Screen 2, Condition 27, Hampton Research).

632 For data collection the crystals were rapidly soaked in the mother liquor solution (the  
633 crystallization buffer described above) supplemented with 25% glycerol and flash frozen in a  
634 nitrogen gas stream at 95 K. Data were collected at beamline 22BM at the Advanced Photon

635 Source, Argonne National Laboratory equipped with 10Hz Rayonix MX300HS detector. A  
636 crystal that diffracted to 1.97 Å resolution with cell dimensions (in Å) of a =76.66, b =84.32, and  
637 c =132.07 and belonged to the orthorhombic space group I212121 (Table 2) was used to collect a  
638 data set. The data were processed, reduced and scaled with XDS<sup>53</sup>. The structure of CxD7L1 was  
639 determined by molecular replacement using Phaser<sup>54</sup> by employing separate, manually  
640 constructed search models for the N-terminal and C-domains based on the crystal structure of  
641 *Anopheles stephensi* AnStD7L1 (PDB ID: 3NHT). The final model of CxD7L1 was constructed  
642 by iterative manual tracing of the chain using the program Coot<sup>55</sup> after each cycle of refinement  
643 with stepwise increase in the resolution using Phenix<sup>56</sup>. All structural figures were produced with  
644 PyMOL (PyMOL molecular graphics system, version 1.7.4; Schrödinger, LLC) and UCSF  
645 Chimera (Resource for Biocomputing, Visualization, and Informatics at the University of  
646 California, San Francisco, with support from NIH P41-GM103311)<sup>57</sup>.

#### 647 **4.10 Platelet aggregation assay**

648 Platelet rich plasma (PRP) was obtained from normal healthy donors on the NCI IRB approved  
649 NIH protocol 99-CC-0168, “Collection and Distribution of Blood Components from Healthy  
650 Donors for In Vitro Research Use.” Research blood donors provide written informed consent,  
651 and platelets were de-identified prior to distribution. Platelet aggregation was measured using an  
652 aggregometer (Chrono-Log Corporation). Briefly, 300 µL of PRP, diluted 1:3 to approximately  
653 250,000 platelets/uL in Hepes-Tyrode’s buffer (137 mM NaCl, 27 mM KCl, 12 mM NaHCO<sub>3</sub>,  
654 0.34 mM sodium phosphate monobasic, 1 mM MgCl<sub>2</sub>, 2.9 mM KCl, 5 mM Hepes, 5 mM  
655 glucose, 1% BSA, 0.03 mM EDTA, pH 7.4) were pre-stirred in the aggregometer for 1 min to  
656 monitor pre-aggregation effects. Different concentrations of recombinant proteins or TBS as  
657 negative control were added to the PRP before adding the agonists. Aggregation agonists used in

658 our studies included native collagen type I fibrils from equine tendons, convulxin, ADP, U-  
659 46619, arachidonic acid, serotonin, epinephrine, or combination of agonists. Their concentrations  
660 are specified in the figure captions. Technical duplicates were performed.

## 661 **Acknowledgements**

662 We thank Kevin Lee, Andre Laughinghouse, and Yonas Gebremicale for excellent mosquito  
663 rearing and Van My Pham for salivary glands dissection. We also thank John Andersen and Jose  
664 Ribeiro for relevant scientific discussion and Thrity Avary from Chrono-Log Corporation for  
665 technical assistance with platelet aggregation studies. The authors thank Bradley Otterson, NIH  
666 Library Writing Center, for manuscript editing assistance. This research was supported by the  
667 Intramural Research Program of the NIH/NIAID (AI001246-01).

## 668 **References**

- 669 1. Lai CH, Tung KC, Ooi HK, Wang JS. Competence of *Aedes albopictus* and *Culex*  
670 *quinquefasciatus* as vector of *Dirofilaria immitis* after blood meal with different  
671 microfilarial density. *Vet. Parasitol.* **90**, 231-237 (2000).
- 672  
673 2. Simonsen PE, Mwakitalu ME. Urban lymphatic filariasis. *Parasitol Res* **112**, 35-44  
674 (2013).
- 675  
676 3. Cornet S, Nicot A, Rivero A, Gandon S. Evolution of Plastic Transmission Strategies in  
677 Avian Malaria. *PLoS Pathogens* **10**, e1004308 (2014).
- 678  
679 4. Farajollahi A, Fonseca DM, Kramer LD, Kilpatrick AM. “Bird biting” mosquitoes and  
680 human disease: A review of the role of *Culex pipiens* complex mosquitoes in  
681 epidemiology. *Infect. Genet. Evol.* **11**, 1577-1585 (2011).
- 682  
683 5. Turell MJ. Members of the *Culex pipiens* complex as vectors of viruses. *J. Am. Mosq.*  
684 *Control Assoc.* **28**, 123-126 (2012).
- 685  
686 6. Ribeiro JM. Role of saliva in blood-feeding by arthropods. *Annu. Rev. Entomol* **32**, 463-  
687 478 (1987).

688

- 689 7. Ribeiro JM, Charlab R, Pham VM, Garfield M, Valenzuela JG. An insight into the  
690 salivary transcriptome and proteome of the adult female mosquito *Culex pipiens*  
691 *quinquefasciatus*. *Insect Biochem. Mol. Biol.* **34**, 543-563 (2004).
- 692
- 693 8. Valenzuela JG, *et al.* The D7 family of salivary proteins in blood sucking diptera. *Insect*  
694 *Mol. Biol.* **11**, 149-155 (2002).
- 695
- 696 9. Ribeiro JMC, Martin-Martin I, Moreira FR, Bernard KA, Calvo E. A deep insight into  
697 the male and female sialotranscriptome of adult *Culex tarsalis* mosquitoes. *Insect*  
698 *Biochem. Mol. Biol.* **95**, 1-9 (2018).
- 699
- 700 10. Calvo E, Mans BJ, Andersen JF, Ribeiro JM. Function and evolution of a mosquito  
701 salivary protein family. *J. Biol. Chem.* **281**, 1935-1942 (2006).
- 702
- 703 11. Calvo E, Mans BJ, Ribeiro JM, Andersen JF. Multifunctionality and mechanism of ligand  
704 binding in a mosquito antiinflammatory protein. *Proc. Natl. Acad. Sci. U S A* **106**, 3728-  
705 3733 (2009).
- 706
- 707 12. Ribeiro JMC, Arca B. From Sialomes to the Sialoverse: An Insight into Salivary Potion  
708 of Blood-Feeding Insects. *Adv. In. Insect. Phys.* **37**, 59-118 (2009).
- 709
- 710 13. Alvarenga PH, Francischetti IM, Calvo E, Sa-Nunes A, Ribeiro JM, Andersen JF. The  
711 function and three-dimensional structure of a thromboxane A2/cysteinyl leukotriene-  
712 binding protein from the saliva of a mosquito vector of the malaria parasite. *PLoS Biol.* **8**,  
713 e1000547 (2010).
- 714
- 715 14. Jablonka W, Kim IH, Alvarenga PH, Valenzuela JG, Ribeiro JMC, Andersen JF.  
716 Functional and structural similarities of D7 proteins in the independently-evolved  
717 salivary secretions of sand flies and mosquitoes. *Sci. Rep.* **9**, 5340 (2019).
- 718
- 719 15. James AA, Blackmer K, Marinotti O, Ghosn CR, Racioppi JV. Isolation and  
720 characterization of the gene expressing the major salivary gland protein of the female  
721 mosquito, *Aedes aegypti*. *Mol. Biochem. Parasitol.* **44**, 245-253 (1991).
- 722
- 723 16. Conway MJ, *et al.* *Aedes aegypti* D7 Saliva Protein Inhibits Dengue Virus Infection.  
724 *PLoS Negl. Trop. Dis.* **10**, e0004941 (2016).
- 725
- 726 17. Girard YA, *et al.* Transcriptome changes in *Culex quinquefasciatus* (Diptera: Culicidae)  
727 salivary glands during West Nile virus infection. *J. Med. Entomol.* **47**, 421-435 (2010).
- 728

- 729 18. Reagan KL, Machain-Williams C, Wang T, Blair CD. Immunization of mice with  
730 recombinant mosquito salivary protein D7 enhances mortality from subsequent West Nile  
731 virus infection via mosquito bite. *PLoS Negl. Trop. Dis.* **6**, e1935 (2012).
- 732
- 733 19. Styer LM, Lim PY, Louie KL, Albright RG, Kramer LD, Bernard KA. Mosquito saliva  
734 causes enhancement of West Nile virus infection in mice. *J. Virol.* **85**, 1517-1527 (2011).
- 735
- 736 20. Arcà B, *et al.* A cluster of four D7-related genes is expressed in the salivary glands of the  
737 African malaria vector *Anopheles gambiae*. *Insect Mol. Biol.* **11**, 47-55 (2002).
- 738
- 739 21. Malafronte Rdos S, Calvo E, James AA, Marinotti O. The major salivary gland antigens  
740 of *Culex quinquefasciatus* are D7-related proteins. *Insect Biochem. Mol. Biol.* **33**, 63-71  
741 (2003).
- 742
- 743 22. Chagas AC, *et al.* Simplagrin, a Platelet Aggregation Inhibitor from *Simulium*  
744 *nigrimanum* Salivary Glands Specifically Binds to the Von Willebrand Factor Receptor  
745 in Collagen and Inhibits Carotid Thrombus Formation *In Vivo*. *PLoS Negl. Trop. Dis.* **8**,  
746 e2947 (2014).
- 747
- 748 23. Juhn J, *et al.* Spatial mapping of gene expression in the salivary glands of the dengue  
749 vector mosquito, *Aedes aegypti*. *Parasit. Vectors* **4**, 1-1 (2011).
- 750
- 751 24. Arca B, *et al.* Trapping cDNAs encoding secreted proteins from the salivary glands of the  
752 malaria vector *Anopheles gambiae*. *Proc. Natl. Acad. Sci. U S A* **96**, 1516-1521 (1999).
- 753
- 754 25. Huang Y, Niu B, Gao Y, Fu L, Li W. CD-HIT Suite: a web server for clustering and  
755 comparing biological sequences. *Bioinform.* **26**, 680-682 (2010).
- 756
- 757 26. Ma D, Assumpcao TC, Li Y, Andersen JF, Ribeiro J, Francischetti IM. Triplatin, a  
758 platelet aggregation inhibitor from the salivary gland of the triatomine vector of Chagas  
759 disease, binds to TXA(2) but does not interact with glycoprotein PVI. *Thromb. Haemost.*  
760 **107**, 111-123 (2012).
- 761
- 762 27. Mans BJ, Ribeiro JM. Function, mechanism and evolution of the moubatin-clade of soft  
763 tick lipocalins. *Insect Biochem. Mol. Biol.* **38**, 841-852 (2008).
- 764
- 765 28. Francischetti IM, Ribeiro JM, Champagne D, Andersen J. Purification, cloning,  
766 expression, and mechanism of action of a novel platelet aggregation inhibitor from the  
767 salivary gland of the blood-sucking bug, *Rhodnius prolixus*. *J. Biol. Chem.* **275**, 12639-  
768 12650 (2000).



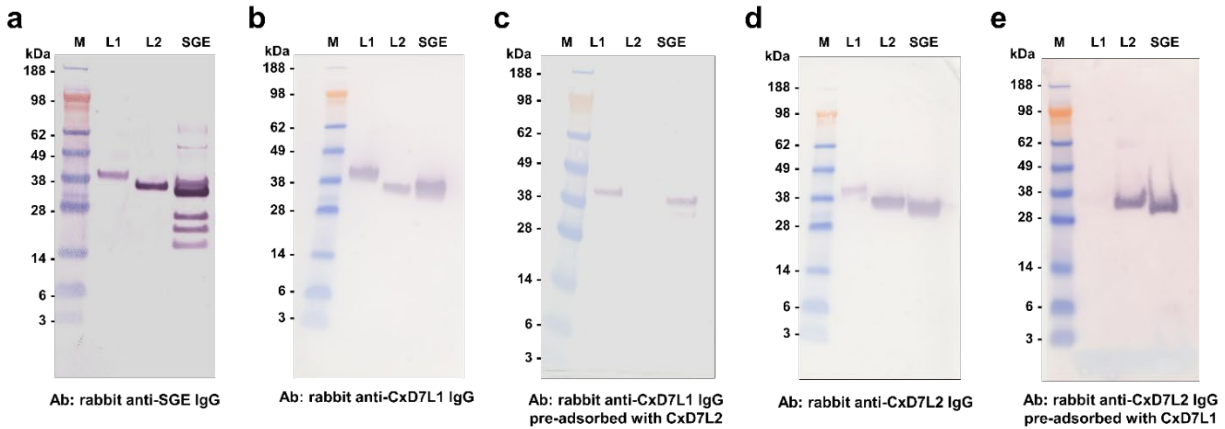
- 769  
770 29. Van Nueten JM, Janssens WJ, Vanhoutte PM. Serotonin and vascular reactivity.  
771 *Pharmacol. Res. Commun.* **17**, 585-608 (1985).
- 772  
773 30. Mans BJ, Calvo E, Ribeiro JM, Andersen JF. The crystal structure of D7r4, a salivary  
774 biogenic amine-binding protein from the malaria mosquito *Anopheles gambiae*. *The J.*  
775 *Biol. Chem.* **282**, 36626-36633 (2007).
- 776  
777 31. Piper PJ. Formation and actions of leukotrienes. *Physiol. Rev.* **64**, 744-761 (1984).
- 778  
779 32. Andrews RK, Berndt MC. Platelet physiology and thrombosis. *Thromb. Res.* **114**, 447-  
780 453 (2004).
- 781  
782 33. Brass L. Understanding and evaluating platelet function. *Hematology Am. Soc. Hematol.*  
783 *Educ. Program* **2010**, 387-396 (2010).
- 784  
785 34. Assumpcao TC, Alvarenga PH, Ribeiro JM, Andersen JF, Francischetti IM.  
786 Dipetalodipin, a novel multifunctional salivary lipocalin that inhibits platelet aggregation,  
787 vasoconstriction, and angiogenesis through unique binding specificity for TXA2,  
788 PGF2alpha, and 15(S)-HETE. *J. Biol. Chem.* **285**, 39001-39012 (2010).
- 789  
790 35. Xu X, Francischetti IM, Lai R, Ribeiro JM, Andersen JF. Structure of protein having  
791 inhibitory disintegrin and leukotriene scavenging functions contained in single domain. *J.*  
792 *Biol. Chem.* **287**, 10967-10976 (2012).
- 793  
794 36. Andersen JF, Francischetti IM, Valenzuela JG, Schuck P, Ribeiro JM. Inhibition of  
795 hemostasis by a high affinity biogenic amine-binding protein from the saliva of a blood-  
796 feeding insect. *J. Biol. Chem.* **278**, 4611-4617 (2003).
- 797  
798 37. Puri RN, Kumar A, Chen H, Colman RF, Colman RW. Inhibition of ADP-induced  
799 platelet responses by covalent modification of aggregin, a putative ADP receptor, by 8-  
800 (4-bromo-2,3-dioxobutylthio) ADP. *J. Biol. Chem.* **270**, 24482-24488 (1995).
- 801  
802 38. Marcus AJ, *et al.* Inhibition of platelet function by an aspirin-insensitive endothelial cell  
803 ADPase. Thromboregulation by endothelial cells. *J. Clin. Inv.* **88**, 1690-1696 (1991).
- 804  
805 39. Cattaneo M, Lecchi A, Lombardi R, Gachet C, Zighetti ML. Platelets from a patient  
806 heterozygous for the defect of P2CYC receptors for ADP have a secretion defect despite  
807 normal thromboxane A2 production and normal granule stores: further evidence that  
808 some cases of platelet 'primary secretion defect' are heterozygous for a defect of P2CYC  
809 receptors. *Arterioscler. Thromb. Vasc. Biol.* **20**, E101-106 (2000).

- 810  
811 40. Clemetson KJ. Platelets and primary haemostasis. *Thromb. Res.* **129**, 220-224 (2012).
- 812  
813 41. Nascimento EP, dos Santos Malafrente R, Marinotti O. Salivary gland proteins of the  
814 mosquito *Culex quinquefasciatus*. *Arch. Insect Biochem. Physiol.* **43**, 9-15 (2000).
- 815  
816 42. Ribeiro JM, Charlab R, Valenzuela JG. The salivary adenosine deaminase activity of the  
817 mosquitoes *Culex quinquefasciatus* and *Aedes aegypti*. *J. Exp. Biol.* **204**, 2001-2010  
818 (2001).
- 819  
820 43. Arca B, Ribeiro JM. Saliva of hematophagous insects: a multifaceted toolkit. *Curr. Opin.*  
821 *Insect Sci.* **29**, 102-109 (2018).
- 822  
823 44. Ribeiro JM, Mans BJ, Arcà B. An insight into the sialome of blood-feeding Nematocera.  
824 *Insect Biochem. Mol. Biol.* **40**, 767-784 (2010).
- 825  
826 45. Giraldo-Calderon GI, *et al.* VectorBase: an updated bioinformatics resource for  
827 invertebrate vectors and other organisms related with human diseases. *Nucleic Acids Res.*  
828 **43**, D707-713 (2015).
- 829  
830 46. Ribeiro JM, Francischetti IM. Platelet-activating-factor-hydrolyzing phospholipase C in  
831 the salivary glands and saliva of the mosquito *Culex quinquefasciatus*. *J. Exp. Biol.* **204**,  
832 3887-3894 (2001).
- 833  
834 47. Bult H, Wechsung E, Houvenaghel A, Herman AG. Prostanoids and hemostasis in  
835 chickens: anti-aggregating activity of prostaglandins E1 and E2, but not of prostacyclin  
836 and prostaglandin D2. *Prostaglandins* **21**, 1045-1058 (1981).
- 837  
838 48. Grant RA, Zucker MB. Avian thrombocyte aggregation and shape change *in vitro*. *Am. J.*  
839 *Physiol.* **225**, 340-343 (1973).
- 840  
841 49. Nelson RL, Tempelis CH, Reeves WC, Milby MM. Relation of mosquito density to bird:  
842 mammal feeding ratios of *Culex tarsalis* in stable traps. *Am. J. Trop. Med. Hyg.* **25**, 644-  
843 654 (1976).
- 844  
845 50. Ribeiro JM, Martin-Martin I, Arca B, Calvo E. A Deep Insight into the Sialome of Male  
846 and Female *Aedes aegypti* Mosquitoes. *PLoS One* **11**, e0151400 (2016).
- 847

- 848 51. Kim IH, Pham V, Jablonka W, Goodman WG, Ribeiro JMC, Andersen JF. A mosquito  
849 hemolymph odorant-binding protein family member specifically binds juvenile hormone.  
850 *J. Biol. Chem.* **292**, 15329-15339 (2017).
- 851  
852 52. Chagas AC, *et al.* Collagen-binding protein, Aegyptin, regulates probing time and blood  
853 feeding success in the dengue vector mosquito, *Aedes aegypti*. *Proc. Natl. Acad. Sci. U S*  
854 *A* **111**, 6946-6951 (2014).
- 855  
856 53. Kabsch W. Integration, scaling, space-group assignment and post-refinement. *Acta*  
857 *Crystallogr. D Biol. Crystallogr.* **66**, 133-144 (2010).
- 858  
859 54. McCoy AJ, Grosse-Kunstleve RW, Adams PD, Winn MD, Storoni LC, Read RJ. Phaser  
860 crystallographic software. *J. Appl. Crystallogr.* **40**, 658-674 (2007).
- 861  
862 55. Emsley P, Lohkamp B, Scott WG, Cowtan K. Features and development of Coot. *Acta*  
863 *Crystallogr. D Biol. Crystallogr.* **66**, 486-501 (2010).
- 864  
865 56. Adams PD, *et al.* PHENIX: a comprehensive Python-based system for macromolecular  
866 structure solution. *Acta Crystallogr. D Biol. Crystallogr.* **66**, 213-221 (2010).
- 867  
868 57. Pettersen EF, *et al.* UCSF Chimera-a visualization system for exploratory research and  
869 analysis. *J. Comput. Chem.* **25**, 1605-1612 (2004).
- 870  
871  
872

873 **Supplementary material:**

874 **Supplementary Fig. 1:**



876 **Supplementary Fig. 1: Recognition of recombinant CxD7L1 and CxD7L2 by IgG antibodies raised in rabbits.**

877 (a) Purified IgG from serum of a rabbit immunized with salivary gland extract (SGE) from *Culex quinquefasciatus*

878 recognized the recombinant proteins CxD7L1 and CxD7L2 (100 ng) and other protein bands from the salivary

879 gland extract (2.5 µg). (b) Purified IgG from serum of a rabbit immunized with CxD7L1 protein recognized

880 CxD7L1 recombinant protein (100 ng) and a band of similar molecular weight in the SGE (2.5 µg). It also cross-

881 reacted with CxD7L2. (c) Purified IgG from serum of a rabbit immunized with CxD7L1 protein and pre-adsorbed

882 with CxD7L2 specifically recognized CxD7L1 recombinant protein (100 ng) and a band of similar molecular weight

883 in the SGE (2.5 µg). (d) Purified IgG from serum of a rabbit immunized with CxD7L2 protein recognized CxD7L2

884 recombinant protein (100 ng) and a band of similar molecular weight in SGE (2.5 µg). It also cross-reacted with

885 CxD7L1 (e) Purified IgG from serum of a rabbit immunized with CxD7L2 protein and pre-adsorbed with CxD7L1

886 specifically recognized CxD7L2 recombinant protein (100 ng) and a band of similar molecular weight in the SGE

887 (2.5 µg). No cross-reactivity between anti-CxD7L1 IgG and anti-CxD7L2 IgG was observed after anti-CxD7L1 was

888 pre-adsorbed with CxD7L2 and anti-CxD7L2 was pre-adsorbed with CxD7L1. Anti-Culex SGE IgG antibodies

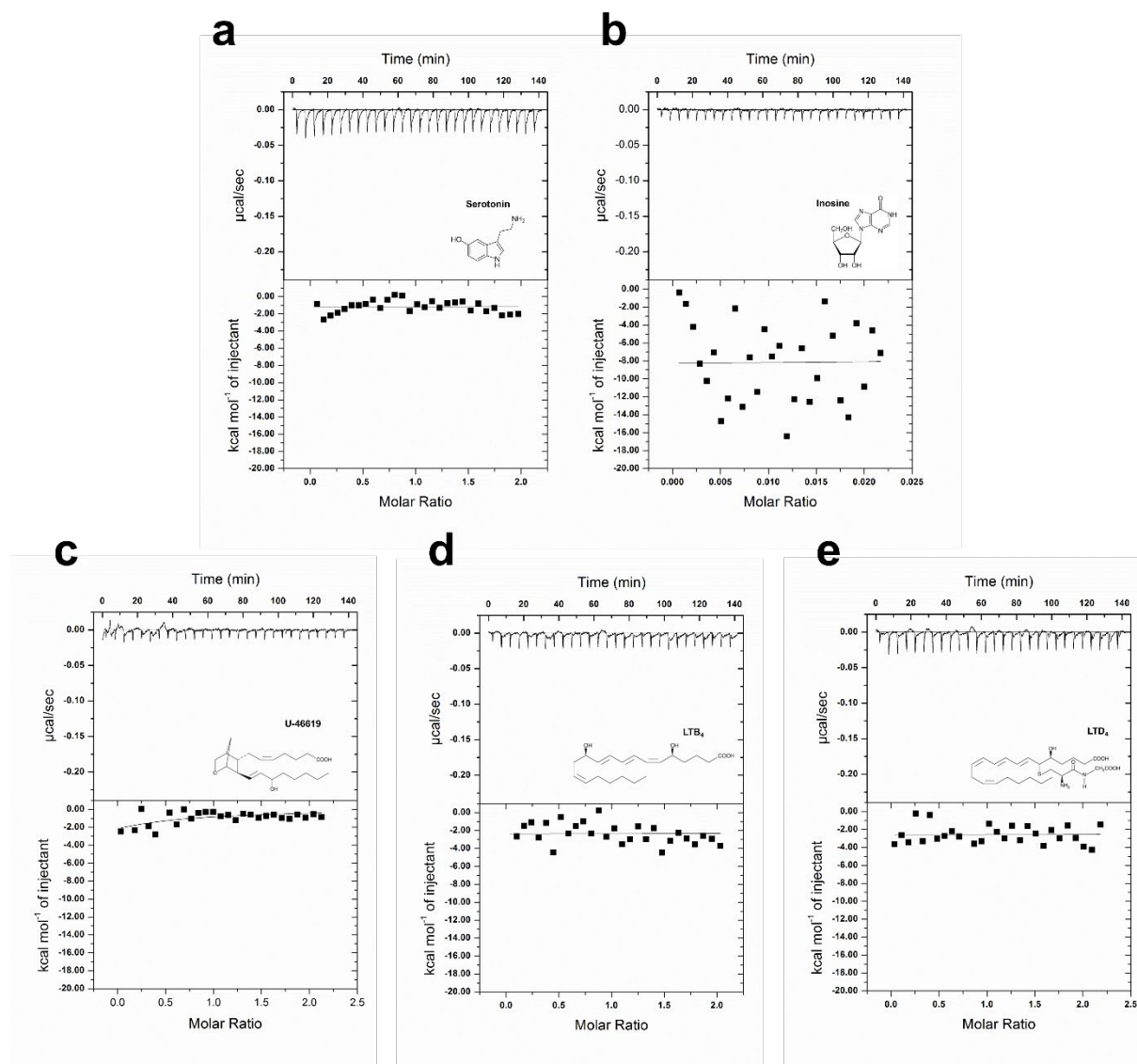
889 were used at 1 µg/ml and IgG antibodies against recombinant proteins were used at 0.5 µg/ml. Goat anti-rabbit IgG

890 AP (1:10,000 dilution, Sigma) was used as a secondary antibody. SeeBlue Plus2 Pre-stained was used as the protein

891 standard (M).

892

893 **Supplementary Fig. 2:**



894

895 **Supplementary Fig. 2. Isothermal titration calorimetry studies of CxD7L1.** Binding experiments were  
896 performed on a VP-ITC microcalorimeter. (a) 30 µM serotonin or (b) 30 µM inosine were titrated with 3 µM of  
897 CxD7L1. For TXA<sub>2</sub> analog U-46619 (c) and leukotrienes LTB<sub>4</sub> (d) and LTD<sub>4</sub> (e) protein and ligand were prepared  
898 at 5 µM and 50 µM, respectively. Assays were performed at 30 °C. The upper curve in each panel shows the  
899 measured heat for each injection, while the lower graph shows the enthalpies for each injection and the fit to a  
900 single-site binding model for calculations of thermodynamic parameters. The insets show the names and chemical  
901 formulas for these compounds.

902 **Supplementary Fig. 3:**

```
CxD7L1_AAL16046.1 1 ----MK---ALF-FLGAI-----IAGVLSDENSPDPEEVAEEAKC
Ctar_JAV19160.1 1 ---MNSRVAVLVTVLQAVCIWSAAVPACDDSSQPAADPSSWIPRNPEQTMAYVRC
Ctar_JAV18819.1 1 -----SKLL-SLTON-----KCPNQTAMKPLDPEQVLEGFSSRC
Ctar_JAV29109.1 1 MDKMPVTVVVALLLIS-----VNQSLASLAFDPEETREVLVRC
Ctar_JAV19100.1 1 ----MNLISITG-LLIVA-----FFTGGNAQMKFPNPEETLEFYTRC
JAV19156.1 1 -----M---KKI-VVLLA-----FGGIVSGOWSPNPEEVAEEQAKC

CxD7L1_AAL16046.1 35 MEDHFGND-----FGLAEKWKWKSIAES--DGTKACYVKCLVEALGMYDKQ--AFQFN
Ctar_JAV19160.1 58 IINDSTAS-----VEQKIRWRWQPPAS---TESQCYVKCVSEELRFLVHERRRFPE
Ctar_JAV18819.1 34 GEDH----TPNDENRTIRIQNMAQWKLPEV--DNWPMCVQCCLEKGLFNVTTKKEMTD
Ctar_JAV29109.1 42 TEQYSTPVSDDSSRQARIRDWESWKLDAAGDEQPKCFVACLINKLEKLPYLCGFQGE
Ctar_JAV19100.1 38 MEDNAKGD-----MELAKKWNWKLK-Q--DPKSAQYAKCVLGLDFDESSRTFAGD
Ctar_JAV19156.1 34 MEDHFKDD-----FTVAEQWLDWKLAKG--DPKTPCYVKCLAEALGLYDDQAKAFQFN

CxD7L1_AAL16046.1 84 NIKQOYENYKSDNGVQTKGDAIENELGKID-AGKGCESIAKGEIQVNNANKGWLEKLY
Ctar_JAV19160.1 107 RFVHQAETVYGRGDVNGELDKLRINAQKPLAGSIEEVTCTETVFNKATFYATHTEHLKMF
Ctar_JAV18819.1 88 HINSOYEGEKKYNEINLTQVNEFATALNSFGEI--HSCADVFRRLTVELKQHMLTLIKLRF
Ctar_JAV29109.1 102 QLEHCHHLYNSYVNWSRADVEEFARAVEQTCGV--WNCQAVVEGKVAIILPQMVWFKQLF
Ctar_JAV19100.1 88 HLEHOYQKYSYTTQEBAGKKEQNAWQALGSWESSDCLKVLOKAPVHAKYTDQPNVY
Ctar_JAV19156.1 85 NINQOYENYKSDNGVPAKABAIQKELEKID-VKGGKCESIGKGLKVESANQGLKRLY

CxD7L1_AAL16046.1 143 LLDSSVREDAVYKK-NPQIKPKGHSIFRFCKQCFYDQG-EAAYCNVRRHG-FSDDPKFIKH
Ctar_JAV18819.1 146 NCSPRINTKLEDELGPTIRORKOSYVEFCENLELKN-KIIVCNFRLRKQRTDGHMKQL
Ctar_JAV29109.1 160 LLEDEIAGNIYADLGTSSIRQPNOSYFCFCERMYRNQ-VDIQCTARNYS-IPDRNFRKH
Ctar_JAV19100.1 148 FGGKKEITLKIYVST-DSLVKKEDEIMFFCFEESNEDQG-SAELECTLRKTC-IITKN---EH
Ctar_JAV19160.1 167 HGDHRDLMETYGLKDKVKTICEFVAVCEKRRGGSWNEDEASP-----ATAL
Ctar_JAV19156.1 144 LIDSAVKDAIYKK-NPQIKPKGHSIFRFCKQCFYDQG-EAAYCNVRRHG-YSDDEKFIKH

CxD7L1_AAL16046.1 200 SNCTTRGRMWMKKNGEDESAILRGLHVAENNGKDDVVKKSLONCKRAKLE-SKARDYYKC
Ctar_JAV19160.1 215 VDCVLRGERWITEEGENVVNEIRRDYAAAGFSDSDSEASCTS-----A---AGARDLEQC
Ctar_JAV18819.1 205 IDCFKGERYLDKEEKDABEIRDFHAGKTKLDDDTQMTLINCFKESQPSAQNYVDC
Ctar_JAV29109.1 218 MDCLFRGIRYEDRDEALNVVEILRDEHLEAVTNLDDEITNSLVLEVESG-SEALSYVRC
Ctar_JAV19100.1 202 IDCLFRGIRYMDRNGNINPAEIKRDLHFNVNDKDDAVDNAENNCVNEA-TKARDYVDC
Ctar_JAV19156.1 201 SNCTTRGRMWMKKNGEDESAILRDLHVAEENSKDDVVKKSLONCKRAKLE-TKARDYYKC

CxD7L1_AAL16046.1 259 IYDGLG--EQIFMKVLDYIEVRSSENYRYLREATS-KYDANAIRSKVQALDSEAKC----
Ctar_JAV19160.1 266 IRLGTLADGATRLNQVIRENRORAFYFDATSQEEF-WRSVAVFQQRMNLI-----
Ctar_JAV18819.1 265 IMSSEKL-EKFFQAADYREFRSSDYDAFAIPEPPIYDCHQVAAAKKRIIALDCN---
Ctar_JAV29109.1 277 ILDSENFV--EQFKDADLYREIRSIDYFHLRDRSVP-SYNRDEHQ-KVNEIHRNYCIMAK
Ctar_JAV19100.1 261 LMKDPNL-KDMMBEVFDYREVRSESYRYFHE-HTE-PYDATKVKKVKYDQDAGC----
Ctar_JAV19156.1 260 IYDGLG--EQIFMKVLDYIEVRSSENYGFRLRKETS-KYDESAVETKVDLDIAKCPVVA

CxD7L1_AAL16046.1 -----
Ctar_JAV19160.1 -----
Ctar_JAV18819.1 -----
Ctar_JAV29109.1 -----
Ctar_JAV19100.1 -----
Ctar_JAV19156.1 317 HGSKK
```

903

904 **Supplementary Fig. 3. Multiple sequence alignment of *Culex quinquefasciatus* CxD7L1 and *Culex tarsalis* D7**

905 **long proteins.** Eighteen D7 homologs from *C. tarsalis* were retrieved from NCBI database after a tBLAST search

906 using the CxD7L1 protein as the query sequence. The database used was the Transcriptome Shotgun Assembly,

907 BioProject PRJNA360148. *Culex tarsalis* sequences with E value lower than 4e-10 were chosen (N = 10) and

908 clustered by [cd-hit software](#)<sup>25</sup> where sequence identity cut-off was set at 0.85. CxD7L1 (AAL16046) and 5

909 representative of *C. tarsalis* D7 long protein homologs (JAV19160, JAV18819, JAV29109, JAV19100, and

910 JAV19156) were aligned with Clustal Omega and refined using BoxShade server. Black background shading

- 911 represents identical amino acids (50% of sequences must agree for shading) while grey shading designates similar
- 912 amino acids. Residues highlighted in blue indicate conserved amino acids involved in ADP binding.